Force Spectroscopy

Wormlike chain

$$F(x) = \frac{k_B T}{\ell_P} \cdot \left[\frac{1}{4} \cdot (1 - x/L)^{-2} + x/L - \frac{1}{4} \right]$$

DNA

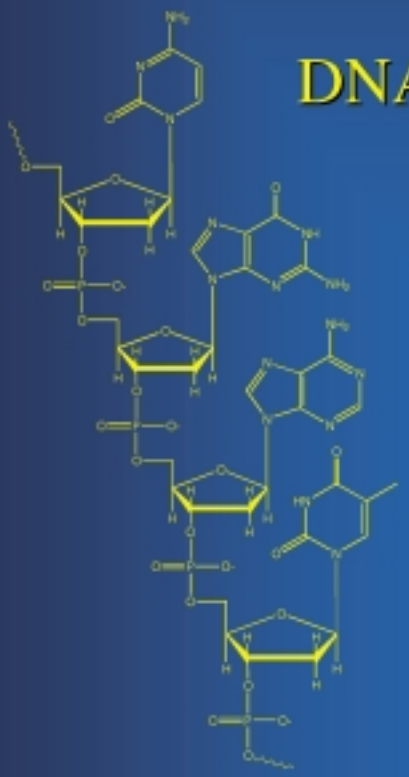

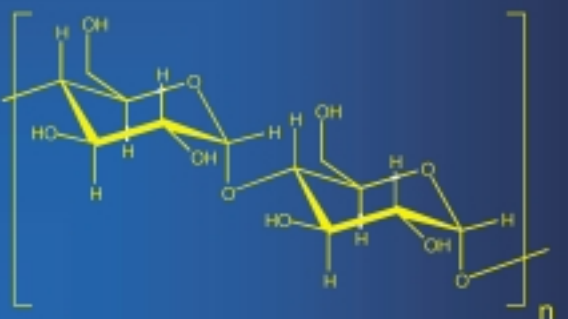

Amylose

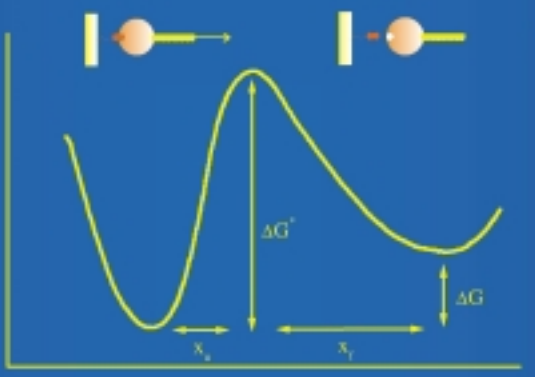

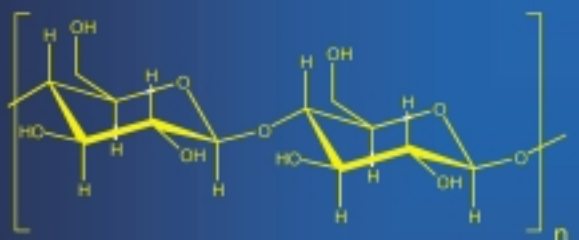

Cellulose

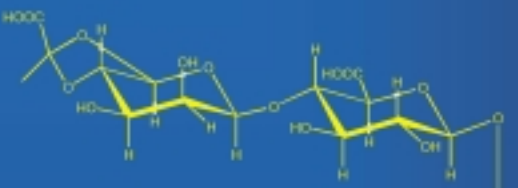

Xanthan

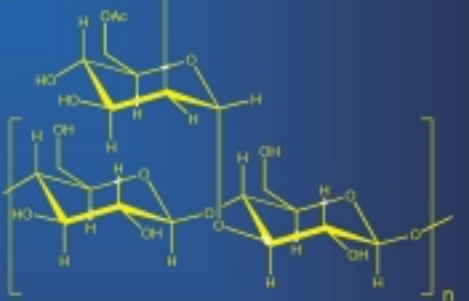

Polypeptides

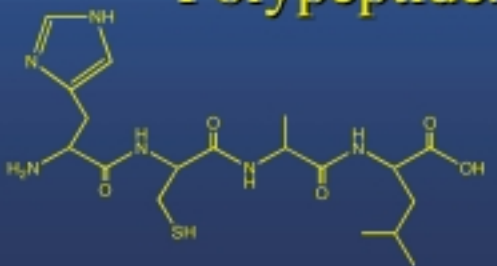

Force Spectroscopy of Molecular Systems—Single Molecule Spectroscopy of Polymers and Biomolecules

Andreas Janshoff, Marcus Neitzert, York Oberdörfer, and Harald Fuchs*

How do molecules interact with each other? What happens if a neurotransmitter binds to a ligand-operated ion channel? How do antibodies recognize their antigens? Molecular recognition events play a pivotal role in nature: in enzymatic catalysis and during the replication and transcription of the genome; it is also important for the cohesion of cellular structures and in numerous metabolic reactions that molecules interact with each other in a specific manner. Conventional methods such as calorimetry provide very precise values of binding enthalpies; these are, however, average values obtained from a large ensemble of molecules without knowledge of the dynamics of the molecular recognition event. Which forces occur when a single molecular couple meets and forms a bond? Since the development of the scanning force microscope and force spectroscopy a couple of years ago, tools have now become available for measuring the forces between interfaces with high precision—starting from colloidal forces to the interaction of single molecules. The manipulation of individual molecules using force spectroscopy is also possible. In this way, the mechanical properties on a molecular scale are measurable. The study of single molecules is not an exclusive domain of force spectroscopy; it can also be performed with a surface force apparatus, laser tweezers, or the micropipette technique. Regardless of these techniques, force spectroscopy has been proven as an extraordinary versatile tool. The intention of this review article is to present a critical evaluation of the actual development of static force spectroscopy. The article mainly focuses on experiments dealing with inter- and intramolecular forces—starting with "simple" electrostatic forces, then ligand–receptor systems, and finally the stretching of individual molecules.

Keywords: DNA recognition · force spectroscopy · polymers · scanning probe methods

1. Introduction: Microscopic Forces

Geschrieben steht:
Im Anfang war der Sinn.
Bedenke wohl die erste Zeile,
dass deine Feder sich nicht übereile!
Ist es der Sinn,
der alles wirkt und schafft?
Es sollte stehn:
Im Anfang war die Kraft!

Johann Wolfgang von Goethe (1749–1832), *Faust I*

The physical unit of force is named after Sir Isaac Newton (1643–1727), who was the first to mathematically describe the concept of force precisely in his axioms. Moreover, Newton was not only interested in long-range gravitational forces but also—ahead of time—in microscopic forces: "The parts of all homogeneal hard bodies stick together very strongly. I had rather infer from their cohesion, that their particles attract one another by some force…". To the best of our present knowledge, Newton already referred to intermolecular forces at that time. The radius of action of intermolecular forces is in the microscopic range, and extends from a few micrometers to several angstroms. Intermolecular forces determine the properties of gases, behavior of colloidal solutions, growing of crystals, and interaction of biomolecules. It is not only the radius of action of these forces which is on the microscopic scale but also its magnitude relative to the forces that are present in daily life. In general, its magnitude is only some fractions of a nanonewton. The direct measurement of such forces is an experimental challenge and was first possible in the late 1970s with the invention of the *surface force apparatus* (SFA).[1] This apparatus can be used to monitor forces between two transparent, atomically smooth and curved mica surfaces covered with the system under investigation by optical interference techniques. The SFA has a force resolution of approximately 10 nN and a vertical resolution of

[*] Prof. Dr. H. Fuchs, Dr. A. Janshoff, Dr. M. Neitzert, Y. Oberdörfer
Physikalisches Institut
Westfälische Wilhelms-Universität
Wilhelm-Klemm-Strasse 10, 48149 Münster (Germany)
Fax: (+49) 251-8333602
E-mail: fuchsh@nwz.uni-muenster.de

  1433-7851/00/3918-3213 $ 17.50+.50/0

0.1 nm. A drawback of this method is its limitation to atomically flat transparent substrates and the lack of lateral resolution. In addition, contaminations on the large surfaces may influence the measurements considerably.

With the development of the atomic force microscope (AFM) in the mid 1980s an instrument became available for the first time that was distinguished not only by its enormous force resolution down to the piconewton range but also by its lateral and vertical resolution.[2] Scanning force microscopy gained high significance in research fields where in situ imaging of surfaces with a submicrometer resolution was required, such as in materials and life sciences. The versatility of this method is based on the large number of contrast mechanisms. Besides the topography, elastic moduli, friction coefficients, chemical residues, surface charges, and energy loss during the oscillation of the cantilever can be imaged with high spatial resolution.

The difference between static force spectroscopy and dynamic force spectroscopy is that in the former the interaction between the tip and the sample is calculated from the amplitude signal as well as the frequency and phase shift of the cantilever's oscillation.[3]

By chemical functionalization of the tip the force microscope has developed as a new tool for materials and life sciences. For the first time it was feasible to measure the forces between two individual molecules locally. A milestone in this regard was the direct observation of a single bond rupture of a distinct streptavidin–biotin complex in 1994 as reported


A. Janshoff


M. Neitzert


Y. Oberdörfer


H. Fuchs

Andreas Janshoff was born in 1966. He attended the Westfälische Wilhelms-University (WWU) Münster, where he received a B.S. in Biology and Chemistry. He received his M.S. in 1994 and his Ph.D. in 1997 for studies on the biofunctionalization of gold surfaces and its applications in bioanalytics, which he carried out at the Institute for Biochemistry at the University of Münster under the supervision of Prof. Hans-Joachim Galla. As a postdoctoral fellow, he worked in the group of Prof. M. Reza Ghadiri at the Scripps Research Institute, La Jolla (CA), USA for 1½ years. During this time he worked on scanning force microscopy imaging of lipid membranes. In 1999 he returned to Germany to join the group of Prof. Harald Fuchs at the WWU Münster starting his habilitation in close collaboration with the Institute for Biochemistry (WWU). His research fields include the development of new sensor systems based on micropatterned surfaces, force spectroscopy of extracellular matrix proteins and the application of acoustic resonators to investigate biological relevant questions.

Marcus Neitzert was born in 1967 in Barcelona, Spain. He moved to Germany in 1986 to study Physics at the University of Heidelberg. He worked at the Laboratory for Surface Science and Technology at University of Maine and returned to Germany in 1994 to start his Ph.D. thesis at the Westfälische Wilhelms-University of Münster under the supervision of Prof. Harald Fuchs. He graduated in 1999 with a thesis on the force spectroscopy of biopolymers. Currently, he is working as a scientific journalist for the public relation office of the Deutsche Physikalische Gesellschaft (DPG).

York Oberdörfer was born in 1973 in Hamm-Heessen, Germany. From 1993 to 1999 he studied Physics at the Westfälische Wilhelms-University of Münster. He is currently a graduate student in the group of Prof. Harald Fuchs and his work is concerned with the force spectroscopy of modular proteins and micropatterning of surfaces.

Harald Fuchs, born 1951, studied Physics at the University of Saarbrücken. After his diploma thesis in theoretical physics he worked at the Institute of Physiology of the University of Saarbrücken until 1980 on transport processes in biological membranes. He graduated in 1982 in the group of Prof. Gleiter at the University of Saarbrücken with a Ph.D. thesis on nanocrystalline systems. Until 1984 he worked as a research associate at the Institute of Material Science. During his postdoctoral stay at IBM Rüschlikon from 1984 to 1985 he worked in the group of Binnig and Rohrer on scanning tunneling microscopy. From 1985 to 1993 he was the head of a research group at BASF AG. In 1993 he became full professor for Experimental Physics at the Westfälische Wilhelms-University of Münster and the head of the institute in 1998. In 1994 he received the Philip-Morris-award for his outstanding work on nanostructuring. His main research fields are nanotechnology, organic/inorganic interfaces, and the development of new scanning probe microscopy techniques.

independently by the groups of Gaub[4] and Colton.[5] Quasi-static force spectroscopy has become established as a particular technique of single molecule spectroscopy and has now found numerous fields of applications. It should be emphasized that not only static but also dynamic information is available, such as during the separation of a single ligand–receptor couple upon applying an external force with different pulling velocities. From these measurements information about the dynamics of the bond rupture of noncovalent complexes and, thus, about the energy barrier which needs to be overcome during bond rupture is gathered. Conformational analysis of polymer strands and biomolecules has also been developed as an additional independent research field. Here, long-chain molecules such as DNA, synthetic polymers, polysaccharides, and filamentous proteins experience folding–unfolding cycles upon application of an external force. The characteristic force–extension curves can be utilized to analyze the different conformations of the biomolecules by applying statistic polymer models.[6] In summary, with scanning force microscopy and related techniques, methods are available that allow imaging and spectroscopic characterization of surfaces on a molecular scale as well as the manipulation of single molecules.

2. General Overview: The Force Microscope as a Sensor of Molecular Forces

Since its invention (1986) by Binnig, Quate, and Gerber[2] force microscopy has evolved from being a predominantly imaging technique[7–9] to a method that allows the investigation of molecular forces at interfaces in great detail.[4, 5] The cantilever of the microscope acts as a sensor for the local interaction between the tip and the sample (Figure 1).

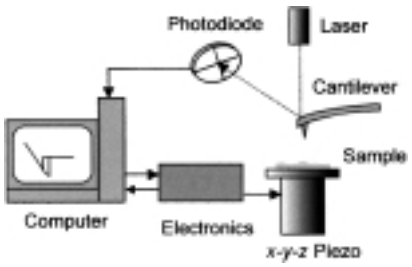

Figure 1. Schematic drawing of a force microscope with a photodetector. The deflection of the cantilever is detected by the laser deflection reflected from the cantilever. The sample is positioned on a piezoelectric device (movable in three directions). The piezo allows the sample to be moved in the vertical direction (z-piezo controlling unit) and scanning the surface in the x-y direction (x-y piezo controlling unit). There are two different modes: in the constant-height mode the cantilever deflection is detected without feedback control (applicable to very smooth surfaces), while in the constant force mode the z-piezo unit compensates for any possible cantilever deflections by changing the z position.

A so-called force–distance curve can be determined by detecting the cantilever deflection[10] (which reflects the dependence of the force on the movement of the piezo device) when the tip of the force microscope is moved toward and away from the surface. The applied force F can be deduced from the cantilever deflection z_F using Hook's law [Eq. (1)]. Force resolution (under ambient conditions) is in

$$F = k z_F \quad (1)$$

the range of piconewtons and restricted to the thermal fluctuation of the cantilever.[11, 12] The entire measurement (approach and withdrawal) typically takes a couple of seconds. In some cases, the retraction curves exhibit various complex features from which conclusions about the interaction between the tip and samples can be drawn (Figure 2). The approach curve also contains valuable information about surface forces.

The interactions observed range from van der Waals forces in the nN scale (Figure 2A) to entropic forces of several hundred pN—the latter ones caused by the stretching of single molecules fixed between the tip and the substrate (Figure 2E). Thus, the interactions occurring are strongly dependent on the experimental conditions, such as the tip and sample material, chemical modification of the surfaces, and the surrounding medium. Therefore, it is in general possible to image surfaces in a chemically sensitive fashion.[13–19] The interactions dominating the course of the experimental force curves depend on the medium. Van der Waals forces, which are always present in air, are in general superimposed by stronger capillary forces, which are caused by the condensation of water vapor in the area where the tip contacts the sample (capillary condensation). These capillary forces are negligible if the measurements are performed in fluids.

Force spectroscopy experiments in an aqueous solution are of major importance since only this environment allows the study of native biological processes and mechanical behavior of single molecules, such as nucleic acids and proteins, in situ. A proper functionalization of the tip and sample is very important for these kinds of experiments. Electrostatic forces are predominant in aqueous solution;[20–23] they can be mainly attractive or repulsive (Figure 2B, C)—depending on the surface potential, the ionic strength, and pH. In addition to electrostatic interactions, the use of molecules with appropriate functional groups leads to short-ranging dipole–dipole interactions, hydrogen bonding,[11, 24–26] or in the case of ligand–receptor couples highly specific complex combinations of different binding types as well as covalent bonding.[4, 5, 27–30]

The forces between the tip and the sample can be investigated by force spectroscopy on a spatially restricted area. The upper limit is given by the contact radius of the tip with the substrate, which is typically of the order of some ten nanometers,[31, 32] while the lower limit is in the range of single molecules or atom groups.

2.1. Force–Distance Curves

The cantilever deflection is a measure of the interaction force. The relationship between the cantilever deflection and the distance between the tip and sample is shown in Figure 3A with $s = l + d - z_F$. As deduced from Equation (1), attractive forces ($F < 0$) lead to a negative cantilever deflec-

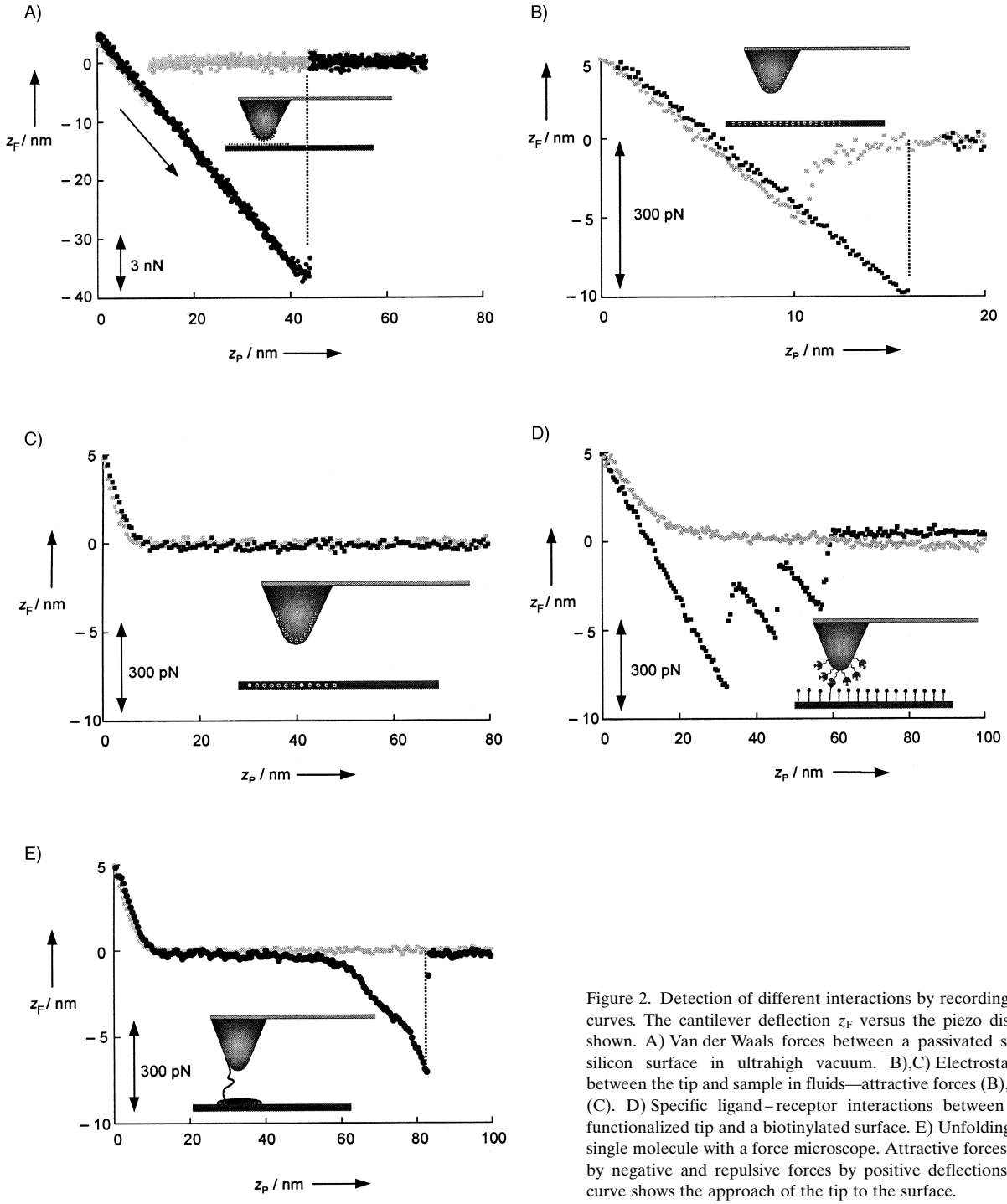

Figure 2. Detection of different interactions by recording force–distance curves. The cantilever deflection z_F versus the piezo displacement z_p is shown. A) Van der Waals forces between a passivated silicon tip and a silicon surface in ultrahigh vacuum. B),C) Electrostatic interactions between the tip and sample in fluids—attractive forces (B), repulsive forces (C). D) Specific ligand–receptor interactions between a streptavidin-functionalized tip and a biotinylated surface. E) Unfolding of a long-chain single molecule with a force microscope. Attractive forces are represented by negative and repulsive forces by positive deflections. The light gray curve shows the approach of the tip to the surface.

tion ($z_F < 0$). For a movement of the sample as a result of the displacement of the piezo device Δz_P, $\Delta s = \Delta z_P$ is valid.[33] From this, the relation $\Delta z_P = \Delta d - \Delta z_F$ follows ($z_F < 0$ at attractive forces and $\Delta l = 0$). The slope of the force curve can be determined from Equation (2), where Δz_F is the change in

$$\frac{\Delta z_F}{\Delta z_P} = \frac{1}{K/F'(d) - 1} \qquad (2)$$

cantilever deflection, and Δz_P is the change in the sample position or displacement of the piezo device. k is the spring constant of the cantilever and $F'(d)$ the force gradient, which is a function of the tip–sample distance d. Equation 2 provides a stability criterion ($k/F'(d) - 1 \neq 0$). The characteristic features of an approach and retraction curve is given in Figure 3 B.

If the tip is far away from the surface forces are absent and the cantilever is not deflected (1). Attractive surface forces become apparent when the tip approaches the substrate: if the value of the positive force gradient is the same as the spring constant ($F'(d) = k$) a mechanical instability occurs according to Equation (2), known as snap-on (2). The tip jumps into a close repulsive contact with the sample (2→3),

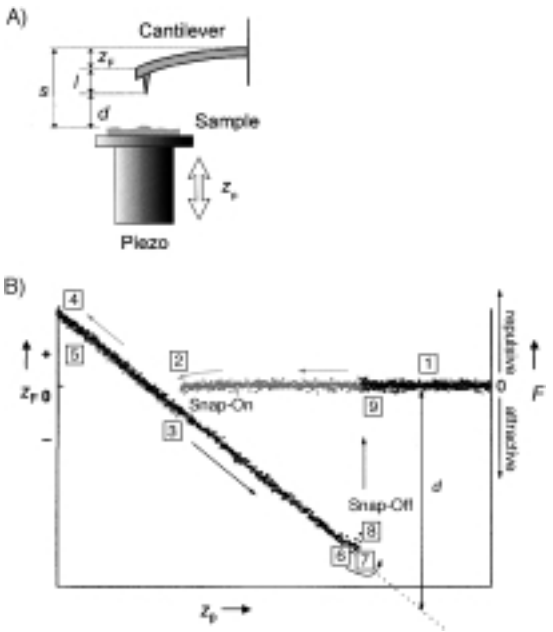

Figure 3. A) Relevant parameters for calculating the transfer function between the sample displacement z_P and the cantilever deflection z_F; l is the length of the tip, d the distance between the tip and the sample. B) Simple force curve; the numbers and arrows illustrate the course of the measurement. A detailed description is given in the text.

and consequently the surface experiences deformation. Even if the cantilever was infinitely stiff, a snap-on would always be present on the atomic scale, since the gradient of the surface forces becomes larger than the elastic restoring force at any small separation (1–2 Å).[34] Although the net force is negative, repulsive forces also act on the cantilever.[35] The deflection of the cantilever (3→4) is now determined by the viscoelasticity of the substrate.[36] Applications of force microscope range from the measurements of deformation of elastomers[37] or thin organic layers[38] to mechanical experiments on individual cells.[39] A quantitative determination of the elastic moduli is, however, difficult in most cases as the contact area needs to be known precisely.[40, 41] This is rarely the case since on the one hand the tip geometry varies from cantilever to cantilever and on the other hand the contact radius is a function of adhesion.

The pressure that the tip exerts on the surface increases as the sample displacement increases. In the case of a hard substrate ($|F'(d)| \gg k$) the slope of the force curve converges to -1 (4), sample displacement and cantilever deflection are proportional ($\Delta z_P = -\Delta z_F$, here $z_P = -z_F$). The distance between the tip and the sample remains constant along this contact line. For example, this is the case for glass and passivated silicon. This fact is used to calibrate the cantilever deflection in the case of force microscopes using a laser deflection signal, which means that the deflection is directly obtained from the signal of the photodiode (voltage).

The repulsive forces decrease continuously (5→6) upon retraction of the z-piezo device. The separation from the sample surface occurs at the so-called snap-off (8), which is visible immediately after the minimum of the curve (7)—at this point the maximum attractive force can be measured (adhesion force). According to the most common contact models[37, 42] the adhesion force F_{Adh} is proportional to the tip radius and the surface energy between the tip and the sample. The snap-on and the snap-off are both characterized by a mechanical instability ($F'(d) = k$); the contact to the sample surface is suddenly interrupted (8→9). The cantilever reacts sensitively to disturbances, such as thermal noise or vibrations, in the vicinity of the curve minimum (7). Therefore, the snap-off already occurs at the minimum. Large regions of the attractive interaction potential are not accessible experimentally because of the snap-on and snap-off. This becomes more pronounced for softer cantilevers. Under appropriate conditions the adhesion force, that is, the snap-on/off, might vanish in fluids. The interaction between the tip and the sample is then mainly repulsive.

A force curve is a plot of the measured force versus the displacement of the z-piezo device. The spring constant has to be determined most accurately for a quantitative evaluation of the force. A very elegant method of calibrating is to monitor the spectral density of the thermal noise of the cantilever. The determination of the average amplitude of the vibrational resonance allows the calculation of the spring constant.[43] In most cases it makes more sense to display the force as a function of the tip–sample distance. The displacement of the piezo device can be translated into a tip–sample distance by subtracting the contact line from the cantilever deflection[44]—after this normalization one obtains a so-called force–distance curve. It is possible to directly determine persistence and contour lengths of polymers and elasticities of single-molecule chains from the tip–sample distance.[45]

The approaching and retracting path of a force curve does not necessarily match (hysteresis). The enclosed area reflects the energy that is transferred from the cantilever to the sample and the environment during the entire cycle. The hysteresis is a measure of the viscosity of the sample. The sample gains deformational energy during the snap-on. If the sample is retracted and the tip is still on the surface, mechanical energy is stored in the strain of the cantilever. When the tip jumps off the surface, the energy is mainly transformed into vibrational energy of the cantilever.

3. Interactions Between the Tip and the Sample

3.1. Forces in a Vacuum

Van der Waals forces act between all particles on a nanometer scale. They emerge from the interplay of permanent and induced or fluctuating dipole moments and exhibit a $1/r^6$ distance dependency for two pointlike particles. The interaction between identical particles in a vacuum is always attractive. Van der Waals forces between different particles embedded in a third medium might also be repulsive.[20, 37] A single van der Waals bond is relatively weak and of the order of -1 kJ mol^{-1}, which is equivalent to approximately 10 meV per molecule.[20]

The interaction energy between macroscopic bodies such as a tip and a sample, that is, a sphere–plate model is given for small distances d between the sample and tip [Eq. (3)]:[46] H is

$$W(d) = -HR/6d \quad (3)$$

the conventional Hamaker constant (a typical value in a vacuum is $H \approx 10^{-19}$ J[20]). Figure 4 shows numerical simulations of the interaction of a silicon tip with a silicon sample in ultrahigh vacuum. The tip–sample interaction $F(d)$ that is needed for the numerical simulation of the force curve was determined following the approach of Muller–Yushchenko–Derjaguin/Burgess–Hughes–White (MYD/BHW). This model describes the entire course of the potential. The starting point is again the van der Waals force.[47] The interfacial energy of the composite (Si/SiO_2) can be estimated from the obtained adhesion force to be $\gamma \approx 90\ mJ\,m^{-2}$. This value is in the range expected for van der Waals forces. The interfacial energy of approximately 1200 $mJ\,m^{-2}$[48] for pure silicon is larger since covalent bonds can be formed through dangling bonds.[49]

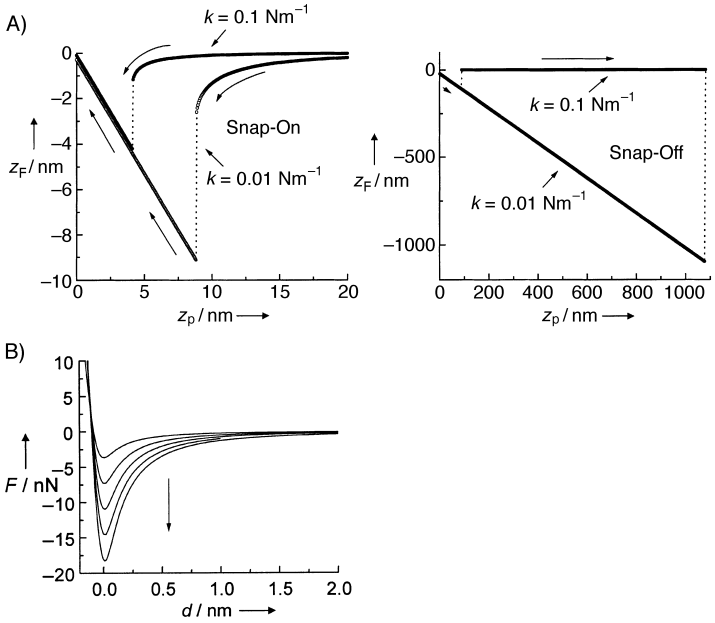

Figure 4. Influence of the spring constant and the tip radius on the appearance of the force–distance curve. A) Simulated force plots (sample approach) using different spring constants k (MYD/BHW potential, tip radius $R = 30$ nm). B) Interaction of a silicon tip with a silicon substrate according to the MYD/BHW theory (based on van der Waals forces).[3] Elastic modulus $Y = 179$ GPa, Hamaker constant $H = 2.5 \times 10^{-19}$ J. An increase of the tip radius R (arrow) leads to a deeper potential with longer range.

3.2. Forces in Air

The predominant adhesive force in air is the capillary or meniscus force. A distinct hysteresis between the approach and retraction curve can be observed in the experimental force curve; during the approach the adhesion force is considerably larger than other attractive forces. The adhesion force is approximately 10–100 nN and is therefore the prevailing force. In principle, the capillary force depends on the surface tension of the sample, tip, and fluid as well as on the tip radius, air humidity, and the thickness of the water layer. Quantitative measurements are mostly performed in a vacuum, a dry gas atmosphere, or directly in liquids. Besides the dominating capillary forces, Coulombic forces may occur if a voltage is applied between a conductive tip and sample. These forces are mainly used to determine the geometry of the tip.[50]

3.3. Electrostatic Forces in Aqueous Solutions

Van der Waals forces are weaker in aqueous solution than in a vacuum.[20, 51, 52] This fact is the result of the high dielectric constant of water ($\varepsilon \approx 80$)—van der Waals forces are of electrodynamic origin and are thus shielded from water dipoles. Though weak, van der Waals forces among particles of the same kind in nature are always attractive, even in electrolytes. Colloidal particles aggregate and precipitate as long as van der Waals forces are present. However, dissolved particles carry charges on their surface, which leads to repulsive forces that prevent aggregation. For example, red blood cells have negative surface charges that protect them from agglutination.[53]

These electrostatic forces are dependent on the ion concentration and the pH of the solution. In simple terms, the pH influences the surface charge, while the number of ions in solution affects the radius of action of the electric field. Figure 5 depicts schematically the course of the potential at an interface. Electrostatic interactions among charged surfaces in fluids can be classically treated with the Poisson–Boltzmann equation,[54] which describes the potential and charge density of the counter ions at every spot x except for the surface.

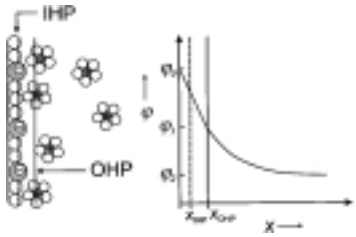

Figure 5. Left: Schematic drawing of the electrochemical double layer according to Stern. The first part of the double layer (Helmholtz layer) is characterized by a linear decrease in the potential up to the outer Helmholtz plane (OHP) followed by the diffuse double layer (Gouy–Chapman layer). The separating line at the inner Helmholtz plane (IHP) is positioned at the center of specifically adsorbed ions (here negatively charged). Ions carrying a solvation shell can approach the electrode only up to the outer Helmholtz plane because of the finite extension of the adsorbed ions. The graph on the right-hand side depicts the potential in the corresponding regions.

The theory of Derjaguin, Landau, Verwey, and Overbeck (DLVO)[20, 52, 54] deals with the interplay of electrostatic interactions (which result from the charge distribution described above) and short range van der Waals forces. Only once the surface force apparatus was established could a number of the occurring surface forces be experimentally investigated, such as attractive van der Waals forces, repulsive electrostatic double-layer forces, solvation and structural forces, hydration forces, steric interactions, and hydrophobic

forces. Such interactions have also been shown by force spectroscopy experiments to be present in electrolytes.[21, 22, 55–59]

The force F resulting from the approach of charged surfaces (namely, the tip and the sample) as a function of the distance d reads to a first approximation (for $d > \kappa$) as Equation (4).[21, 60] ϕ_s and ϕ_P are the surface charges on the tip and sample,

$$F(d) \propto \phi_S \phi_P \exp(-d/\kappa) \quad (4)$$

respectively, and κ the Debye length, which is a measure of the range of the electric field[61] or the extension of the electrostatic double layer.[54] The situation is rather complex and depends on the surface charge.[62] For the symmetric case, that is, the overlap of two identical double layers, there is a repulsive (long-range) interaction, whose origin is not electrostatic.[63] In such a situation an electrostatic interaction would always favor an association. In reality, the effect is of entropic nature. The dissociation of surface molecules and the release of ions in solution result in a gain in entropy. Upon approaching the two double layers these ions are pushed (against the entropy) back to the surface. Consequently an osmotic pressure becomes generated—a repulsive force becomes apparent.

The DLVO theory describes the entire interaction as a superposition of the exponential repulsion and the attractive van der Waals force. Hence, the van der Waals interaction dominates at small distances below approximately 5 nm.[64] If the Debye length decreases because of an increase of the ion concentration the long-range repulsion also decreases and the interaction becomes overall attractive.

When nonequally charged surfaces come close together[52, 65, 66] the interaction is either repulsive or attractive depending on the ratio of the charges. If the charges are equal but opposite, the interaction is attractive. Figure 6 shows the

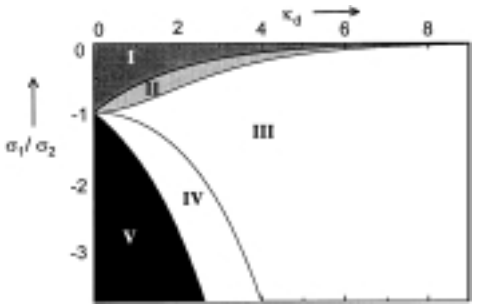

Figure 6. Regions of attractive and repulsive forces as a function of the Debye length κ_d and the ratio of the charge density σ_1/σ_2 of the approaching surfaces.[62] I: Repulsion with both surface potentials positive; II: attraction with both surface potentials positive; III: attraction with surface potentials of different signs; IV: attraction with both surface potentials negative; V: repulsion with both surface potentials negative.

different areas of attractive and repulsive interactions occurring between planar and oppositely charged surfaces. Long-range electrostatic interactions can be monitored spatially resolved using force microscopy. Here, the pioneering work dealing with force spectroscopy at electrochemical double layers was performed by Butt et al.[21, 53, 67] They demonstrated for the first time the influence of pH and ionic strength on the surface potential using scanning force microscopy. Figure 7 shows the dependence of the force curves obtained experimentally on the ionic strength for a silicon nitride tip approaching a self-assembled film of 3-sulfanylpropionic acid

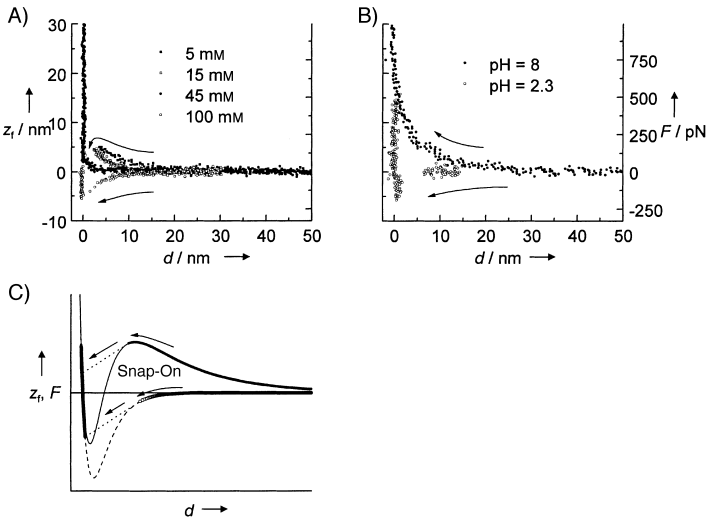

Figure 7. Analysis of electrostatic interactions by means of force–distance curves (only the approach curves are shown). A Si_3N_4 tip in contact with a self-assembled film (3-sulfurylpropionic acid) at pH 7.7: the tip and sample are both negatively charged. A) Variation of the ion concentration (KCl): repulsion is clearly observable before snap-on in the approach curve. Long-range electrostatic repulsion is well resolved at low ion concentrations. At 45 mM, snap-on occurs very close to the surface and the jump-to-contact is not resolved. B) Variation of the pH at low ion concentrations: at pH 8, both the tip and sample are negatively charged, which results in repulsive interaction; whereas at pH 2.3 the interaction is attractive. C) Numerical simulation of force–distance curves (qualitative) with underlying interaction forces (assuming a superposition of van der Waals forces and exponential repulsion) for low (——) and high ion concentrations (- - - -).

chemisorbed on gold.[68] At concentrations of 100 mM KCl the Debye length is already so small that attractive van der Waals forces prevail, and therefore the attraction is discernable (Figure 7A). A numerical simulation supports this result (Figure 7C). Likewise, the dependence of the surface charges on the pH value of the solution is shown. If both surfaces are negatively charged (pH 8), repulsion is predominant at an ionic strength of 5 mM. At pH 2.3, attraction is favored. Surface potentials can be imaged and surface charges, for example, of biomembranes, such as the purple membrane of the halobacterium *Halobacterium salinarium*, can be determined with this method.[67]

3.4. Solvation Forces

If two surfaces approach as close as a couple of nanometers the forces occurring cannot be sufficiently ascribed with continuum theories, such as attractive van der Waals and repulsive double layer forces. Short-range forces resulting from the molecular structure of the fluid are summarized to so-called solvation or structural forces.[20] The geometric organization of the solvent molecules at the solid surface

plays a crucial role in the strength of these forces. The attractive forces between the solvent molecules and the solid surface lead to an organization of the molecules into quasidiscrete layers. In the case of a fluid enclosed between two solids, one can show that rearrangements are induced as those two surfaces approach, which in most cases provide an exponential decay of an oscillating force. Monotonously declining attractive or repulsive components can also occur, and these are dependent on the geometry of the molecule and the interaction potential with the surface. A special case of the solvation force is the repulsive hydration force observed in aqueous solution. It describes the force necessary to remove the hydration shells of surface-confined molecules and bring the tip closer to the surface. In the case of two approaching lipid bilayers composed of zwitterionic phospholipids, very short-range forces of entropic nature with a range of 1 – 2 nm are observable because of the overlap of the head groups and hydrophobic chains. Forces which occur from the adsorption of highly charged ions can be determined from those hydration forces caused by steric effects. Butt demonstrated that an exponentially decaying repulsive force with a decay length of approximately 3 nm occurs if one eliminates the classical double-layer repulsion by adding $CaCl_2$ or $SrCl_2$.[69]

3.5. Chemical Force Microscopy (CFM)

This concept is a particular case of force spectroscopy where the tip and the substrate are derivatized so that interaction between defined functional groups can be clearly distinguished. In general, the immobilized molecules are low molecular weight compounds which in most cases contain only one functional group so that the interpretation of the results is facilitated.[13, 14] The topics that can be addressed by CFM range from the spatially resolved determination of surface energies to locally determined pK values, which are obtained by mapping adhesion forces. Functionalization is mostly achieved by covering the tip and sample surface with gold and subsequently chemisorbing thiolated molecules. As an alternative, classical silane chemistry using mono- and trialkoxysilanes or trichlorosilanes is utilized. The environment (atmosphere, electrolyte concentration, pH) plays a central role in CFM. The following sequence of adhesion forces between amine- and carboxy-terminated functional groups was determined by force spectroscopy in a dry gas atmosphere to be in accordance with their binding strength: $COOH/NH_2 > COOH/COOH > NH_2/NH_2$.[70] There is a vast number of data available for different interactions in various organic solvents, water, and gases. The interested reader is referred to the comprehensive review article of Noy et al.[70]

Adhesion forces are generally larger among functional groups that have the ability to form hydrogen bonds than those without. Force spectroscopy is of particular interest if high surface energies need to be determined, such as which occur with carboxylic acid monolayers, which cannot be determined conventionally by contact angle measurements.

Mechanical models are the theoretical foundations for calculating surface energies using adhesion forces.[71] In 1881 H. Hertz described the deformation of two elastic spherical bodies; however, adhesion was not considered.[72] An analytical contact model including adhesion was developed by Johnson, Kendall, and Roberts (JKR model).[73] To simplify this model it is assumed that adhesion is established by surface energy implying only forces in close contact to the surface. Derjaguin, Muller, and Toporov (DMT model) postulated a distance-dependent potential.[74] For the sake of simplicity they assumed, that deformation of the surface is, apart from external forces, dependent on adhesion forces, which can be determined by integrating the energies of all the atoms in one body with all the atoms in the other. A complete solution of the contact problem of two elastic adhesive bodies is given by the MYD/BHW model.[75] In the first case, the surface forces are, for example, described by a Lennard – Jones potential. A consequence of the MYD/BHW-model is that the pull-off force is dependent on the elasticity of the contact body and is in between the limits of the DMT and the JKR model. Depending on the elasticity of the body and the attractive forces a mechanically stable (DMT model) or a "jump to contact" behavior (JKR model) is conceivable.[3]

In most cases the JKR or DMT model is sufficient to describe the experiment. While the JKR model is well suited for modeling soft and very adhesive bodies with large radii the DMT model describes bodies with the opposite properties best. From both the JKR and DMT model, a direct proportionality between adhesion force and adhesion energy can be obtained if a spherical tip and a flat surface is assumed: W_{ad} ($F \propto R W_{ad}$), with $W_{ad} = \gamma_{SM} + \gamma_{TM} - \gamma_{ST}$. γ_{ST}, γ_{TM}, and γ_{SM} are the free surface energies with the following indices M: medium, S: sample, and T: tip, and R is the radius of the tip. Large adhesion forces result from large interaction energies between the tip and the sample. To obtain γ_{ST}, first the tip and the sample are functionalized equally and γ_{TM} and γ_{SM} determined at the same time. Afterwards, γ_{ST} can be obtained by measuring the adhesion force between the tip and the sample when they are differently functionalized.[76]

The free surface energy reflects the ionization state of the surface-confined molecules. Thus, the dependency of the state of the surface charges on the pH of the solution can be determined using contact angle measurements that lead to the pK values of the functional groups on the surface. These values can also be obtained using adhesion force measurements with appropriately functionalized CFM tips, especially if high surface energies need to be determined and contact angle measurements fail. A titration of the adhesion forces of a COOH-functionalized tip and sample is shown in Figure 8.[70] The obtained surface pK value of approximately 5.5 agrees well with those determined in solution, which indicates that neighboring group effects can be neglected.

The basis for determining surface energies in the fashion described above are macroscopic models, which do not consider the discrete nature of the contact problem. If large forces occur, spontaneous rearrangements on the atomic scale and plastic deformations, which already occur at low forces, play a crucial role. Moreover, the assumption of an ideal

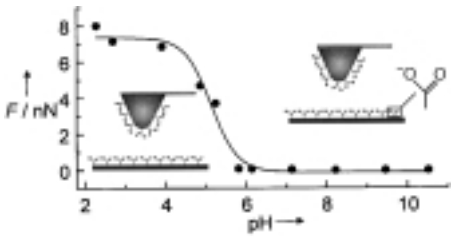

Figure 8. The dependence of the adhesion force F between a tip functionalized with 3-sulfanylpropionic acid and a similarly prepared substrate on the pH of the solution. At the point where the pH = pK of the immobilized carboxylic acid the adhesion force decreases, since deprotonation abolishes formation of hydrogen bonds and as a consequence adhesion declines.[70]

smooth surface as required by contact models is not fulfilled in reality. Even an insignificant roughness of some nanometers diminishes the adhesion considerably.

4. Force Spectroscopy of Ligand – Receptor Interactions

Molecular recognition of biomolecules plays a pivotal role in nature. Ligand – receptor interactions occur during the formation of double-stranded Watson – Crick DNA, in enzymatic reactions, in antigen – antibody recognition events, hormone – receptor reactions, signal transduction, the initial step of the infection of viruses and bacteria, inflammatory reactions, muscle function, adhesion and migration of cells, and in the cohesion of the cytoskeleton. Binding forces are generally a combination of electrostatic, hydrophobic, dipole – dipole interactions, and hydrogen bonding and depend on the conditions such as pH and ionic strength. Besides the thermodynamic and kinetic data, the complex interplay of forces is of paramount interest for the understanding of structure – function relationships of biomolecules.

For example, the consequences of simple point mutants (exchange of a single amino acid) on the specificity and binding strength of proteins can be investigated. Force spectroscopy is complementary to established methods which measure the properties of large ensembles of molecules. It is possible to estimate the shape of the potential describing the transition from the bound to the free state by means of statistical analysis of binding/rupture events. Accompanying the experiments, molecular dynamics (MD) simulations provided various supporting information that facilitated the understanding of binding and rupture on a molecular level.[77] Evans and Richie, for example, managed to close the gap between MD calculations and experiments of dynamic bond dissociation under an external force by means of Monte Carlo simulations.[78]

A typical experiment to investigate molecular recognition events comprises the functionalization of the probe (namely, the tip) and substrate with their respective binding partners. Here, it is important that the binding of the molecule to the tip or sample is much stronger than the intermolecular bonding being investigated. Two techniques dominate the chosen approaches, the chemisorption of thiols on gold and silanes on siliconoxide surfaces. These covalent or quasi-covalent bonds ensure that the weakest bonds are the noncovalent ones between the biomolecules. Cross-linking between anchor molecules and various biomolecules can be achieved by common bioconjugation chemistry such as through the formation of amide bonds or imines. A contact between the sample and the tip is accomplished by moving the z-piezo device with the mounted sample towards and away from the tip. Retraction with constant velocity provides the desired information about bond-rupture events. Modern instruments permit complete control during these approach and retraction cycles through the sweep velocity, duration the tip is in contact, and resolution. Retraction is usually accompanied by several distinct rupture events. It is most probable that the last rupture event under an external force is the breakage of one single bond, since only then are few connections between the molecules left. Ideally, only one single bond of the ligand – receptor pair ruptures.

Statistical analysis of the data obtained shows the number of rupture events versus rupture force. By definition, the maximum peak represents the binding strength. Distributions occurring at higher binding forces can also be meaningful if the maxima are described in terms of nF (a multiple n of the actual binding force F, see Figure 13B—the shoulder at 556 pN represents the simultaneous rupture of two bonds). Coincident breakage of several bonds results in multiples of the binding force.[97]

It should be noted that as an alternative approach, the binding strength can be resolved by applying the Poisson distribution as introduced by Beebe and co-workers. This approach enables the binding rupture to be analyzed without resolving single rupture events.[79]

A simple kinetic model can be used to explain basic observations in force experiments, such as the probability distribution of rupture forces and their dependency on retraction velocity. The model is also successful in describing the force-driven unfolding of polymers, as will be described in more detail in Section 5).

4.1. Kinetics of Ligand – Receptor Separation

The lifetime of noncovalent bonds in the absence of external forces is considerably high. However, pulling long enough at one or the other end with an external force may eventually overcome the potential barrier arising from thermal fluctuations, and thus break the bond. The following presentation will show that adhesive and cohesive forces do not only depend on binding enthalpy but also on the pulling velocity. From a chemical point of view pulling a ligand – receptor couple apart can be considered as an infinite dilution of both compounds. The system is far away from thermal equilibrium and from a kinetic viewpoint the rate constant of association is negligible. Only the rate constant of dissociation is meaningful, the probability of rebinding is zero. The binding strength is thus a result of the kinetic stability of the corresponding complex. Binding strength depends on the pulling velocity relative to the thermal equilibrium conditions. As the external force decreases, the potential of the barrier,

dissociation that occurs on the time-scale of the experiment, is a result of thermal fluctuations. Bell introduced a simple model of binding dissociation under external forces that was based on the transition-state theory.[80] He assumed that the free enthalpy of the transition state ΔG^* is reduced by the external force $\Delta G^* - Fx_u$, in which F denotes the mechanical, external force and x_u the width of the potential of the bound state.

Figure 9 illustrates the two-state model which allows the basic observations made in force spectroscopy to be explained. In analogy to radioactive decay or a monomolecular

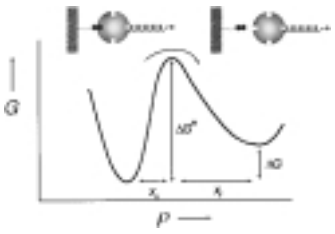

Figure 9. Classic two-state model of bond rupture of a ligand–receptor couple (left diagram) and the unfolding of a polymer (right diagram). ΔG^* is the free activation enthalpy, which is reduced by an external force until bond rupture occurs as a result of thermal noise, ΔG is the binding enthalpy, x_u the width of the potential of the bound state, and x_f the potential width of the unbound state.

reaction the probability of bond breakage after time t can be expressed by Equation (5), where k_{off} denotes the rate constant of dissociation. Notably, the rate constant depends, in

$$p_{off} = 1 - \exp(-\int_0^t k_{off}(t')\mathrm{d}t') \quad (5)$$

contrast to classical kinetics, on the time t [Eq. (6)]. x_u represents the dependence of the distribution of rupture

$$k_{off} = \nu_0 \exp\left(-\frac{1}{k_B T}(\Delta G^* - \int_0^{x_u} F(t)\mathrm{d}x)\right) = \alpha \exp\left(\frac{Fx_u}{k_B T}\right) \quad (6)$$

forces on the shape of the potential, ν_0 denotes the frequency of the bond (the reciprocal of a diffusive relaxation time), and α denotes the dissociation rate in the absence of external forces. The time-dependence arises from the external force given by $F(t) = kvt$, in which v is the pulling velocity and k the spring constant of the cantilever.

Equation (6) illustrates that the rate of dissociation increases exponentially with the external force and therefore with the pulling velocity of the cantilever, whereas the association rate decreases exponentially with the external force. The probability density w that bond rupture occurs under an external force ramp is given in Equation (7). $w(F)$ describes the frequency of rupture events for a particular

$$w(F) = \frac{\mathrm{d}p_{off}}{\mathrm{d}F} = \frac{\alpha}{kv} \exp\left(\frac{Fx_u}{k_B T}\left(\frac{k_B T}{kvx_u}\alpha\left(1 - \exp\left(\frac{Fx_u}{k_B T}\right)\right)\right)\right) \quad (7)$$

force and is usually illustrated by a histogram. By definition the maximum of the distribution is identical to the rupture force of the binding [Eq. (8)]. Increasing the pulling velocity results in a shift of the distribution to higher binding forces as shown in Figure 10.

$$F = \frac{k_B T}{x_u} \ln\left(\frac{x_u}{k_B T \nu_0} kv\right) + \frac{\Delta G^*}{x_u} \quad (8)$$

The width of the distribution depends on the width of the potential x_u and the thermal energy. A more elaborated description of this issue is given by Evans and Ritchie.[78] Bell lumped the whole energy topology in one single parameter x_u, while Evans and Ritchie proposed a model in which bond breakage can be either classified as ductile or brittle. When the frictional losses arising from intrinsic and hydrodynamic damping are considered the rate of dissociation can be expressed as Equation (9), in which $g(F)$ and $\Delta\Delta E^*(F)$

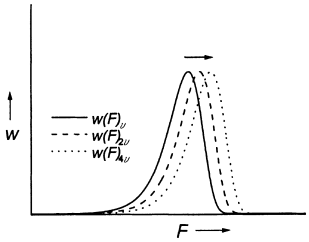

Figure 10. Numerical simulations of the probability density w as a function of the applied force F at three different pulling velocities (increasing in the direction of the arrow). According to Equation (7), the rupture force increases logarithmically with the pulling velocity.

$$k_{off} = \alpha g(F) \exp\left(-\frac{\Delta\Delta E^*(F)}{k_B T}\right) \quad (9)$$

represent the deformation of the potential under the influence of the external force and molecular friction, respectively. Hence, increasing the pulling velocity results in a shift in the distribution of the probability density to higher binding forces and is accompanied by a broadening of the function.

4.2. Hydrogen Bonding and Complementary DNA Strands

Among the vast number of molecular recognition events in nature the base pairing of the DNA duplex is the most recognized one. Colton and co-workers were the first to describe an experimental approach using force spectroscopy to determine the binding strength of a DNA duplex by using single-stranded DNA immobilized on a probe and sample.[81] Silica beads with 60–120 nm diameters were derivatized with trimethoxysilanes and covalently linked to oligonucleotides with the sequence $(ACTG)_5$ (tip) and $(CAGT)_5$ (sample). In this way 20, 16, 12, 8, and 4 base pairs could be formed theoretically. Lee et al.[24] found four populations with force maxima at 1.52, 1.11, 0.83, and 0.48 nN. The adhesion force between noncomplementary base pairs was determined to be merely 0.38 nN. Thus, the obtained forces correspond to the breakage of double stranded DNA with 20, 16, and 12 base pairs (the maximum at 0.48 nN was ascribed to a nonspecific interaction). The pulling velocity varied between 0.1 and 10 nm s^{-1}. In addition, C_{20}-single strands immobilized on the tip and sample were connected through poly(I)-single-strands with different lengths (Figure 11).[81]

Lieber and co-workers determined the binding strength of complementary DNA strands (14 bp) to be 0.45 nN. The nonspecific adhesion force was 0.1 nN.[82] Boland and Ratner chose a more general approach to directly quantify the binding strength of single base pairs such as adenine and thymine as well as cytosine and guanine.[83] Their starting point was a well-ordered self-assembled film of the corre-

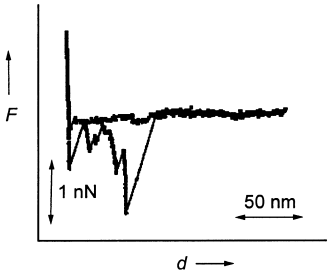

Figure 11. Force-induced rupture of double-stranded DNA. The surface was functionalized with cytidine (C_{20}) and hybridized using poly(I). The tip was also derivatized with C_{20}, so that the bridging of both cytosine single strands with poly(I) becomes possible during the approach.[81]

sponding sulfuranyl derivatives of adenine (A), cytosine (C), thymine (T), and 2-amino-6-hydroxy-8-sulfuranylpurine (G), a guanine analogue, on crystalline gold. They studied the interaction with the corresponding bases immobilized on the tip and 16 combinations were quantified with respect to the attractive forces occurring during the approach. An average attractive force of 0.63 nN for the base-pair A-T and 1.08 nN for G-C was obtained from the approach curve, whereas the rupture forces on retraction were 3.24 nN for A-T and 3.10 nN for G-C (different nonspecific adhesion forces were also identified). It was shown that the distribution of the attractive forces display increments of 54 pN, which is indicative of the formation of single hydrogen bonds. A simple estimation yields 125 pN for the A-T base-pair by assuming an enthalpy of 1.8 kcal mol^{-1} for hydrogen bonds and a base separation of 0.2 nm. The calculation becomes more cumbersome when the weaker Hoogsten base-pairing, which occurs between AA, GG, CC, TT, and AG, is taken into account. Florin et al. observed a dependence of the adhesion forces on the duration of contact between a poly-dT-functionalized tip and a poly-dA-coated sample.[84] The maximum of adhesion was reached after a contact time of 2 min. This can be explained in terms of the slow reorientation of partially hybridized DNA double strands.

Recently, Rief et al.[85] reported on the rupture of single-stranded hairpin loops consisting of alternating A-T and G-C sequences; They found values of 9 pN for the A-T sequence and 20 pN for the G-C sequence. In the course of the experiment the strands melted, which was induced by the external force enabling the molecule to adopt a hairpin conformation. The rupture of the hairpin loop takes place in quasi-thermal equilibrium (reversible) and is thus independent of the duration of the applied force. This observation implies that formation of base pairing and rupture occurs faster than the approach – retraction cycle of the force measurement. A similar time-range was found by Essevaz-Roulez et al. for the unfolding of double-stranded DNA (10 – 15 pN).[86]

Strunz et al. investigated the dynamics of the unwinding of complementary DNA strands at different pulling velocities (16 – 4000 pNs^{-1}) under physiological conditions.[87] Both 5′-termini of the double-stranded DNA were linked to the sample and probe through a polyethyleneglycol (PEG) spacer in order to suppress nonspecific interactions in the vicinity of the substrate. Strunz et al. showed that the binding force is dependent on the number of base pairs and scales logarithmically with the pulling velocity according to a simple two-state model. The elasticity of the DNA (about 2 pN nm^{-1}) changes only moderately with increasing numbers of base pairs. The cooperative melting of the DNA duplex also depends on the frequency ν and thus on the number of base pairs, since the degree of freedom increases with an increasing length of the molecule. Strunz et al. demonstrated that the force which is needed to melt DNA converges with increasing length of the duplex to approximately $1.2\,k_bT$/0.7 Å (70 pN). This value is, however, independent of the pulling velocity of the cantilever. In this context, the work of Bockelmann et al. should be mentioned. They discovered the occurrence of sequence-dependent molecular stick – slip motion while separating a DNA double strand.[88, 89] Essevaz et al. estimated the energy (by force spectroscopy) which is necessary to melt λ-phage-DNA to be 1.9 kcal mol^{-1}. This value is in good agreement with classical DNA melting experiments that revealed 1.5 kcal mol^{-1} for the A-T and 3 kcal mol^{-1} for the G-C base-pairs.[90] It should be mentioned that besides hydrogen bonding, base stacking has a considerable influence on the stability of DNA duplexes.

Recently, McKendry et al. showed that the chirality of low molecular weight compounds can be detected sensitively by means of force spectroscopy using a tip functionalized with acetylphenylglycine (T) and a sample coated with mandelic acid (M).[91] Both compounds were immobilized on gold substrates using thiol anchors. The sample was additionally structured by means of microcontact printing. Different combinations of enantiomers and racemic mixtures were quantified with respect to their adhesion forces. The strongest interaction was observed by using the T(*S*)/M(*R*) and M(*S*)/T(*R*) enantiomeric pairs (1.1 nN). The results reveal that local force spectroscopy may become well suited for pharmacological applications (pharma screening).

4.3. Ligand – Receptor Interactions of Proteins

Noncovalent ligand – receptor interactions of proteins are of widespread interest for immunologists, physiologists, and biochemists. Beside gathering information about the different interacting forces, the determination of the overall binding strength can provide valuable data for understanding the interaction of proteins with high and low molecular weight compounds. For example, the consequences of point mutations near the active center can be quantified and the shape of the binding potential may become available. A number of noncovalent ligand – receptor couples such as antigen – antibody, biotin – streptavidin/avidin and P-selectin – glycoprotein have so far been investigated by force spectroscopy (Table 1).

The first experiments on molecular recognition were conducted by the groups of Gaub[4] and Colton,[5] both investigating the streptavidin – biotin system. Figure 12 displays a typical force – distance curve of a streptavidin-functionalized tip retracting from a biotinylated surface (BBSA). Biotin blocks the binding sites of streptavidin in solution, thus no rupture forces are observable.[68]

Particularly interesting are investigations of the force-induced rupture of ligand – receptor bonds in the case of selectin – glycoprotein and –lipid couples because of their significance in the inflammatory response of mammalians. In response to an inflammatory signal, leukocytes in the blood-

Table 1. Binding parameters of antobody – antigen complexes

Complex components	F [pN]	ΔG [kJ mol^{-1}]	v [μm s^{-1}]
IgG (goat), biotinylated BSA[95]	111.5 ± 98.6	–	–
single-chain F_V (wild-type), fluorescein[12]	50 ± 4	-50.8	1
single-chain F_V (His(H58)-Ala), fluorescein[12]	40.3 ± 3	-44.8	1
human serum albumin (HSA), polyclonal anti-HSA[27]	240 ± 48	–	–
biotin, avidin[4, 93, 96]	170 – 280	–	–
streptavidin, biotin[5]	340 ± 120	–	–
Hb-A1c-antibody, anti-Hb-A1c-antibody[97]	278 ± 83	–	< 2
Microniona prolifera (MAF), anti-MAF[30]	50	–	–
adhesion molecule (ICAM-1), anti-ICAM antibody (F10.2)[151]	100 ± 50	–	–

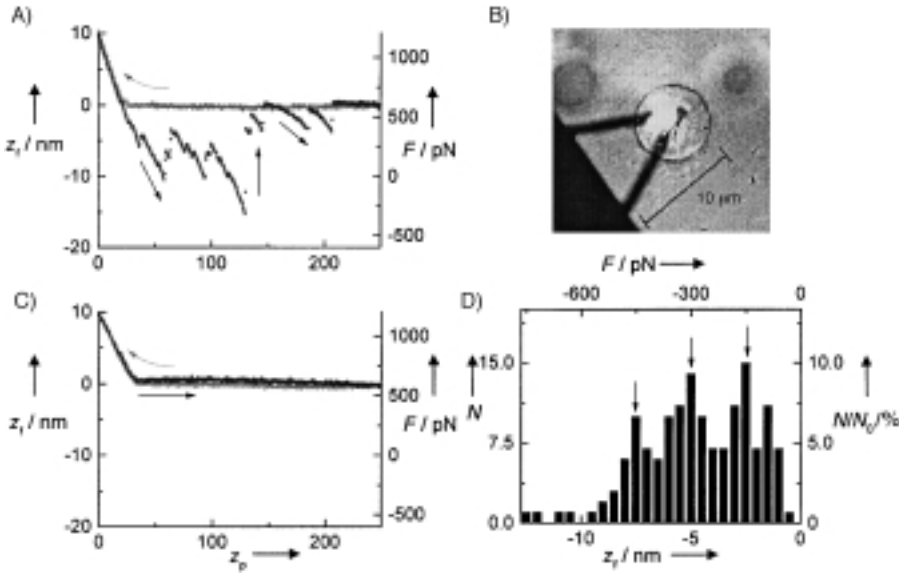

Figure 12. A) Typical force curve of a tip functionalized with streptavidin interacting with a biotinylated substrate. The separation of the tip occurs in several steps in which discrete bonds between the tip and the sample break one after the other. The tip was covered with biotinylated bovine serum albumin (BBSA) and subsequently incubated in a streptavidin solution. Biotinylated agarose beads, adsorbed onto glass, serve as the substrate. B) Optical image of a V-shaped cantilever above an agarose bead. C) Control experiment, in which biotin was added to the solution to block the binding sites of streptavidin. No bond ruptures were observed. D) Histogram of the rupture forces of the biotin – streptavidin couple. In the histogram three maximums separated by a distance of 150 pN are discernible—and correspond to the rupture of one, two, and three ligand – receptor bonds.[68]

stream start to roll on the surface of the endothelia in which adhesion is mediated by selectins produced by the endothelial cells. This movement, generated by an external force, the bloodstream, can be simulated in a force experiment. P-selectin strongly binds to its ligand, the P-selectin-glycoprotein-ligand-1 (PSGL-1), presented by leukocytes. Binding sites are located far away from the cellular membrane at the N-terminus of the polypeptide chains. Fritz et al. studied this system using recombinant fusion proteins with a constant IgG region.[92] Probes (Si_3N_4) and samples (glass) were derivatized by silane chemistry and coated with avidin, which served as the anchor for biotinylated PSGL-1/IgG (tip) and biotinylated P-selectin (sample). The authors managed to determine not only the binding strength of the complex ($F = 110 - 165$ pN), which depends on the pulling velocity of the cantilever, but also the adhesion probability as a function of the duration of contact. It was shown that the binding strength increases logarithmically with the pulling velocity, as expected from the two-state model [Eq. (8)]. In contrast to typical antigen – antibody and streptavidin – biotin reactions the adhesion probability decreases exponentially with interaction time. The width of the potential was 0.25 nm and the rate of dissociation in the absence of an external force 0.022 s^{-1}. A Monte Carlo simulation revealed that rupture forces are mainly determined by the dissociation constant of the complex and scale exponentially with the pulling force [Eq. (8)].[92] However, the association rate is not influenced by the rupture force but by the adhesion probability. The results reveal that the kinetics of the binding/dissociation process are important and binding forces are a function of the pulling velocity. The fact that both binding force and adhesion probability depend on the pulling velocity indicates that the rate constants are in the same timescale as the experimental pulling velocity of the cantilever.

The success of a force experiment depends on two factors, force resolution, which is limited by the thermal noise of the cantilever, and suitable functionalization of the tip and sample. In particular, steric hindrance arising from the immobilization of molecules can lead to considerable differences between binding constants in solution and on surfaces. Therefore, derivatization of the surface must involve flexible spacer molecules and linkers. For instance, the limited mobility of an antibody with a length of merely 10 Å connected directly to the tip can be improved by using spacer molecules, thus increasing the binding probability. Hinterdorfer et al.[27] immobilized the antibody polyclonal anti-human serum albumin (anti-HSA) covalently through a PEG spacer to the probe and measured a binding strength between HSA and anti-HSA of $F = (240 \pm 48)$ pN. Ludwig et al.[93] used a protein cushion consisting of bovine albumin to study the interaction of biotin with avidin which was bound to a biotinylated Si_3N_4 tip derivatized by nonspecifically adsorbed biotinylated bovine albumin (BBSA) in order to avoid denaturing the avidin. They determined a binding strength of $F = 200$ pN for the biotin – avidin complex.[94] Ros et al.[12] used aminopropyltriethoxysilane to couple the antigen fluorescein (Fluor-NHS 5000) to the tip. The authors found a binding force of $F = (50 \pm 4)$ pN and a free enthalpy of $\Delta G = -50.8$ kJ mol^{-1} for fluorescein and single-chain F_V (wild-type) fragments, while single-chain F_V fragments (His(H58)-Ala mutants) displayed a binding strength of $F = (40.3 \pm 3)$ pN and a free enthalpy of $\Delta G = -44.8$ kJ mol^{-1}. Dammer et al. utilized thiol – gold chemistry in conjunction with activated carboxylic

acids to study the binding strength of anti-biotin – immunoglobulins (ABIO) and biotin – BSA.[12, 95]

Besides gold, mica and silicon surfaces have been extensively used as they are atomically flat and can easily be derivatized by silane chemistry.[12, 17] Nonspecific interactions between the molecules on the tip and sample have to be taken into account. Protein-functionalized agarose-beads have been utilized in order to minimize the nonspecific interactions. These polymer beads are known to suppress nonspecific interactions efficiently.[4, 93, 96] Two different types of control experiments are conceivable. Either one prevents binding between the two partners through the addition of an inhibitor to the solution which blocks the binding sites of the receptor, preferably with low molecular weight compounds,[4, 27, 30, 127] or one may remove one binding partner from either surface quantitatively.[1] In either case the maximum of the force spectrum should vanish if it represented a specific interaction. The remaining forces most likely represent nonspecific interactions and result in a background that can hardly be avoided. Examples are given in Figure 13. In this experiment the binding strength of Hb-A1c antibodies has been determined to be $F = (278 \pm 83)$ pN and rupture events were suppressed by adding antibodies to the solution.[97]

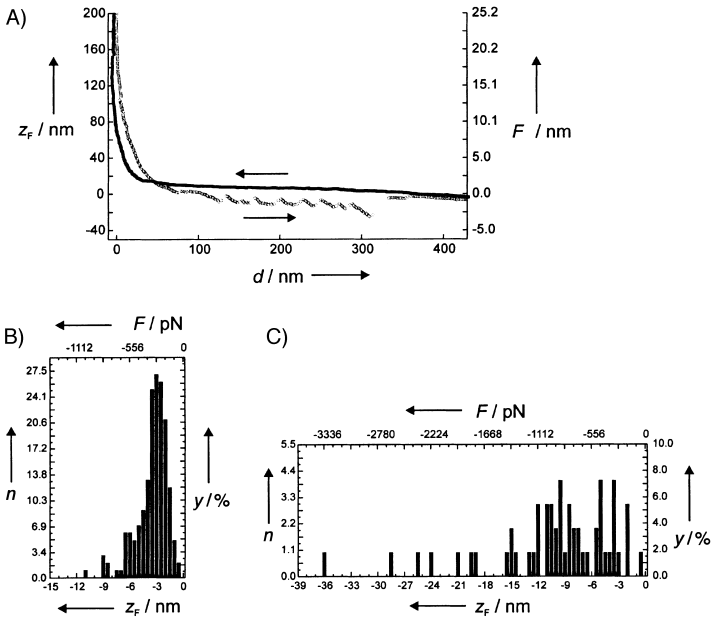

Figure 13. Force curves and the histogram of bond rupture events of an antigen – antibody complex. A) Force curves display the typical picture of a long filament, which is at first stretched and then strips off the tip at a defined force. B) The histogram is composed of 171 curves (171 of 300 force curves exhibited bond rupture events). The number of ruptures (as n and as a percentage of the total number of ruptures (y)) is depicted as a function of rupture length and rupture force. C) Control experiment with a tip in which the antigens were blocked with antibodies from solution. The histogram shows the last ruptures of the force – distance curves, which were obtained with a tip that is blocked with antibodies. Only 55 of 300 curves show rupture events.[97]

Possible changes in binding characteristics that result from the immobilization of proteins on the surfaces have to be taken into consideration if force spectroscopy is performed. Effects range from slight conformational changes up to the entire denaturation of proteins.

4.4. Covalent Bonds

Determining the binding strength of covalent bonds by force spectroscopy is cumbersome and requires caution since the anchoring of the molecules can give rise to a variety of different types of bonding. Although most polymers exhibit only one type of bonding immobilization on the tip and surface adds on several heterogeneous bonds. Either the bond under investigation needs to be the weakest member in the chain or weaker bonds have to be compensated for by designing parallel bonds of the same kind to enhance the strength, as provided by the use of trichlorosilanes and a subsequent cross-linking. So far only one convincing report regarding this difficulty has been published and provides an approach to determine the strength of two types of covalent bonds. Grandbois et al. anchored an amylose chain covalently between the tip and the sample surface and measured the binding strength of the Si–C (2 nN) and Au–S (1.4 nN) bond.[98] The immobilization chemistry was chosen to be identical at the tip and the sample in order to facilitate the analysis of bond breakage. To determine the Si–C bond strength the glass surface and the tip were both functionalized with *N*-(3-trimethoxysilylpropyl)diethylenetriamine, while the carboxymethylated amlyose was activated with 1-ethyl-3-(3-dimethylaminopropyl)carbodiimide (EDC) which would then be covalently linked to the substrate. Contact with the tip gave rise to the desired second linkage to the probe from a molecule suspended between the tip and the sample.

Since amylose exhibits a reversible conformational transition at 275 pN, which is independent of the pulling velocity, the binding forces could be quantified without prior calibration of the cantilevers. The determination of the binding strength of the Au–S bond was performed in the same manner. Activated carboxymethylated amylose was covalently linked to a self-assembled film of cysteamine on gold, while immobilization on the tip was accomplished by silane chemistry as described above. In both cases multiple irreversible ruptures occurred but only a single polymer chain was stretched. From this result one may assume that bond breakage took place at the tip where multiple bonds were formed by the silane anchor. Four conceivable bonds had to be considered: Si–O, Si–C, C–C, and C–N. The authors deduced from computer simulations that the Si–C bonds most likely break, although there is room for speculation about the Au–S bond. It remains to be elucidated whether the Au–S bond ruptures or gold atoms are removed from the substrate and give rise to the observed rupture events.

5. Intramolecular Interactions: Stretching of Single Long-Chain Molecules

The biological function of proteins is directly related to their structure. Polypeptides do not fold randomly but adopt a certain structure based on specific intramolecular interactions. The structure of biomolecules can be studied by circular dichroism spectroscopy, IR spectroscopy, X-ray analysis, and NMR spectroscopy, while their stability can be analyzed by calorimetry. In most cases, the energy hypersurface is

unknown, which makes a direct measure of intramolecular forces necessary. This measurement can be done using force spectroscopy on single molecules. The polymer is immobilized on the substrate and interacts with the tip specifically or nonspecifically. On retraction of the cantilever the molecules are stretched revealing important information about their conformation. The forces of interest are mostly weaker than those associated with bond rupture, thus a special treatment of the probe can be avoided.[45, 99, 100]

Statistically valid results are only obtained if many single-molecule experiments are performed and a large number of experimental data obtained. Combining the data with computer simulation can be very useful in determining a variety of microscopic parameters, for example, mechanical quantities such as the elasticity of the molecule, and the thermodynamic and kinetic parameters such as the energy barrier between the folded and unfolded state as well as between different conformational states of a biopolymer. The following section deals with a general discussion of different polymer models.[101]

5.1. Thermodynamics of Polymers

Even a single polymer chain made up of hundreds to thousands of monomers has to be treated by means of statistical physics because of its large number of degrees of freedom. Since all experiments described here are performed in solution the temperature T can be assumed to be constant—the molecule can be described as a canonic ensemble. How does a molecule react on the pulling force or more precisely, what kind of restoring forces occur?

Stretching a molecule causes two kinds of restoring forces.[102, 103] At small displacements, *entropic* forces dominate. If the polymer adopts a random coil conformation the Brownian molecular motion causes a permanent fluctuation of the molecule. For instance, DNA, a relatively rigid polymer, can be considered as linear on a length scale of 0.05 μm.[102, 104] The force experiment requires long strands of several micrometers thus DNA can be regarded as a random coil.[105, 106, 108] The number of conformations is drastically reduced by extending the molecule. This loss in conformational entropy is reflected in the so-called elastic entropy.[102]

Large displacements leads to a tension of the molecular backbone, in which bonds are stretched in the direction of the pulling force. This effect is called *enthalpic* elasticity.[102, 107] The high external force can cause deformations of bonds[45] and can induce rupture of salt bridges and intramolecular hydrogen bonds, and eventually bring about conformational changes of the entire molecule.[99, 108] This is illustrated by the transition from *B*-form DNA to the *S*-form.[102, 106, 108] Polysaccharides can also change their conformation as a result of high external forces.[45, 99, 109, 110]

Force–distance curves of polymers can be recorded by applying different boundary conditions. It is possible to measure the force necessary to maintain a certain length of the molecule. From a thermodynamic point of view this is an isothermal–isochore process, since the volume represents the length of the molecule and the pressure can be substituted by the force. The other possibility is to provide a constant force and measure the length of the molecule, which is an isothermal–isobar process.[111]

The force F of a polymer stretched in the x direction for an isothermal–isobar process can be expressed independently of the microscopic mechanism as Equation (10).[103] It is decisive

$$F = \left(\frac{\partial A}{\partial l}\right)_T = \left(\frac{\partial U}{\partial l}\right)_T - T\left(\frac{\partial S}{\partial l}\right)_T = -kT\left(\frac{\partial \ln Z_r}{\partial l}\right)_T \quad (10)$$

that the change in the free Helmholtz energy A can also be determined. In this case the derivative is determined under isothermal conditions, in terms of the index T. Z_r is the configurational partition function for a chain with a fixed distance between the ends. The Helmholz energy can be expressed by the internal energy U and the entropy S, which represents the first term of the energetic contribution to the force, the second one shows the influence of the entropic force.[103] Stretching a molecule leads in general to a reduction in the entropy by restricting the number of possible configurations. The derivative of the internal energy plays an important role in the stretching of the molecule as well as in the increase in energy caused by the stretch. From both considerations an attractive—positive—force results. In the purely entropic region only the second term on the right-hand side of Equation (10) remains.[102] It follows that in this case the force is proportional to the temperature.[103]

5.2. Polymer Models from Statistical Mechanics

What does the function $F(x)$ actually look like that determines the force–distance curve? $F(x)$ can be obtained from a mathematical modeling of the real molecule (Figure 14). Among the large number of models[103, 112–116] (Table 2) two general approaches dominate: the freely jointed and the wormlike chain. Prior to the discussion of these models the Gaussian chain, a model valid for low pulling forces, will be described.

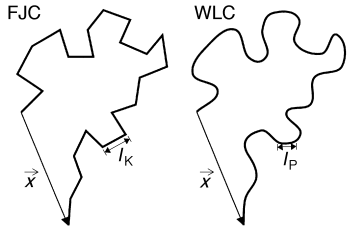

Figure 14. Schematic representation of different polymer models: the freely jointed chain (FJC) is composed of n rigid segments (with the Kuhn length l_K), which are coupled by flexible joints. By replacing the parts of the chain by elastic springs (spring constant κ) enthalpic effects can be included (FJC$^+$). The image on the right-hand side shows the wormlike chain (WLC); it describes the polymer as an irregular curved filament, which is, however, linear on the scale of the persistence length l_P. The introduction of a specific stiffness Φ results in the backbone becoming elastic, that is, stretchable (WLC$^+$). The point to point distance vector $\vec{x}$ connects the starting and the end point of the polymer chain.

Table 2. Elastic models for polymers.

Model	Force law	Fit parameters
freely jointed chain nonelastic (FJC)	$x(F)=L\left[\coth\left(\frac{F l_K}{k_B T}\right)-\frac{k_B T}{F l_K}\right]$	l_x
elastic (FJC$^+$)	$x(F)=L\left[\coth\left(\frac{F l_K}{k_B T}\right)-\frac{k_B T}{F l_K}\right]\left(1+\frac{F}{\kappa L}\right)$	l_K, κ
wormlike chain nonelastic (WLC)	$F(x)=\frac{k_B T}{l_P}\left[\frac{1}{4}\left(1-\frac{x}{L}\right)^{-2}+\frac{x}{L}-\frac{1}{4}\right]$	l_P
elastic (WLC$^+$)	$F(x)=\frac{k_B T}{l_P}\left[\frac{1}{4}\left(1-\frac{x}{L}+\frac{F}{\Phi}\right)^{-2}+\frac{x}{L}-\frac{F}{\Phi}-\frac{1}{4}\right]$	l_P, Φ

5.2.1. The Gaussian Chain (GC)

The conformation of a random coil can be described by a random-walk approach.[117, 118] A Gaussian[102, 103, 112–114] distribution[119] is assumed which is independent of the microscopic structure of the molecule. By assuming an extension x which is smaller than the contour length L of the molecule the random-walk character is preserved. The contour length L is the length of the linearly extended molecule without stretching the molecular backbone.[100, 113, 120] However, a measure for only part of the molecule is usually given for force spectroscopy rather than for the entire length of it.[99] Thus, L represents merely a section of the molecule, since the tip randomly picks up a certain part of the polymer chain.[121] The variable x denotes the distance between tip and sample. By assuming $x \ll L$ the force–distance relationship can be expressed as Equation (11). The force $F(x)$ is a linear function of x and thus the polymer reacts like an ideal spring in the Gaussian model. k_B is the Boltzmann constant and l_K the Kuhn length, which is a measure for the stiffness of the molecule.

$$F(x)=3\frac{k_B T x}{l_K L} \tag{11}$$

5.2.2. The Freely Jointed Chain (FJC)

At higher forces the sections of the chain are no longer oriented in a random fashion and the molecule is predominately aligned along the direction of the external force. This situation can be described by a generic polymer model such as the FJC model. Here, the polymer is divided into n rigid elements, each exhibiting a length of l_K connected through flexible joints without any long-range interactions (Figure 14).

The extension x can be expressed as a function of the pulling force F [Eq. (12)]. $\mathbf{L}$ is the Langevin function[122] and

$$x(F) = L[\coth\left(\frac{F l_K}{k_B T}\right)-\frac{k_B T}{F l_K}] = L\mathbf{L}\left(\frac{F l_K}{k_B T}\right) \tag{12}$$

the contour length is defined as $L=n l_K$. For a large number of segments n, Equation (12)[123] can be written as Equation (13). $\mathbf{L}^{-1}$ is the inverse Langevin function.[124] For small extensions ($x \ll L$) Equation (13) still obeys Hook's law.[125] Large extensions, however, ($x < L$) result in a nonlinear behavior.

$$F(x) = \frac{k_B T}{l_K}\mathbf{L}^{-1}\left(\frac{x}{L}\right) \tag{13}$$

Since the segments of the freely jointed chain are assumed to act independently of each other, the FJC model describes flexible molecules reasonably well. Examples of the successful application of the FJC model are oligonucleotides,[24] polydimethylsiloxane,[126] and poly(methacrylate)[116] (Table 3).

Table 3. Mechanical parameters of different molecules according to the FJC model.

Polymer	Kuhn length [Å]
polyinosine[24] in aqueous solution	3.0
polydimethylsiloxane[126] in heptane	2.5 ± 0.4
polymethacrylic acid[116] in aqueous solution	3.3 ± 0.5

5.2.3. The Extended FJC Model: Combination of Entropic and Enthalpic Elasticity

Both the Gaussian and the FJC models solely consider entropic effects (see Section 5.1). Since elastic deformations are neglected, the polymer chain cannot be stretched by more than the contour length. For large extensions, the Gaussian approach is not valid as the molecules do not behave like an ideal spring. The FJC model also fails to describe the stretching of molecules for $x = L$. According to Equation (13) a molecule would be infinitely rigid at this point. Since this situation is not realistic, one has to take into account deformation of bonds and bond angles. An exact description would require the knowledge of intramolecular potentials and the molecular structure, which in some cases is provided by computer simulations.[45] However, in general one has to choose a generic approach: by modeling the molecule as n identical elastic springs in series the FJC model can be expressed as Equation (14).[108] κ is the spring constant of a

$$x(F) = L\mathbf{L}\left(\frac{F l_K}{k_B T}\right)\left(1+\frac{F}{\kappa L}\right) \tag{14}$$

single segment that can be directly determined by force spectroscopy. Typical values for real polymers are above $1\ \mathrm{N m^{-1}}$. For comparison, the spring constant of the atomic-force microscope is commonly in the range of $0.1-0.01\ \mathrm{N m^{-1}}$. The additional enthalpic term in Equation (14) gives rise to a linear increase in the force for large extensions ($x \sim L$) since the chain behaves elastically. Figure 15 illustrates that the force can be stretched beyond the contour length.

This extended FJC* model has been successfully utilized to describe a variety of different polymers (see Tables 4 and 6) such as polysaccharides,[110] ligand–receptor complexes,[127] as well as synthetic polymers such as polystyrene[128] and polyvinyl alcohol[129] (Table 4).

5.2.4. The Wormlike Chain (WLC)

The model of Kratky and Porod describes a polymer as a homogenous string of constant bending elasticity.[130] The conformation of the molecule can be described as a continuous curve, a wormlike chain. Although entropic *and* enthalpic contributions are combined in this approach,[109] extension is limited by the contour length of the polymer.[131]

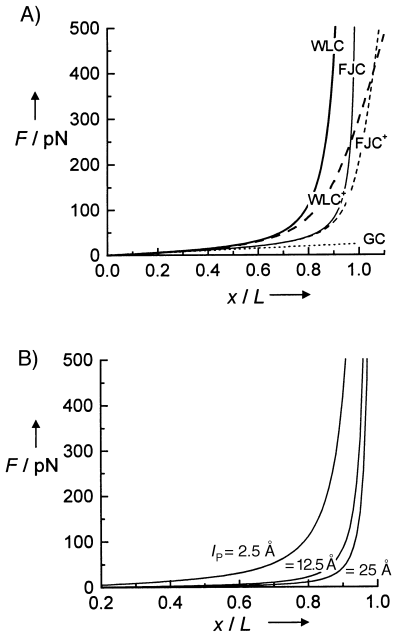

Figure 15. A) Comparison of the force laws of different polymer models: the Gaussian chain (GC), the freely jointed chain (FJC), the wormlike chain (WLC), and the enthalpic extensions FJC$^+$ and WLC$^+$. The significant bending rigidity of the WLC polymer leads to the storing force occurring at lower extensions than in the FJC model. As the individual segments of the FJC polymer can be arranged independently, this chain is extraordinary flexible—upon unfolding of the random coil loops of the polymer strand are evenly stretched without any effort. If the models include a finite stiffness of the segments, then a slower increase in the force occurs at large displacements. This is a result of the elasticity of the chain, which can then be stretched beyond the contour length. Parameters: $T=$ 293.15 K, $l_K = 5$ Å, $l_P = 2.5$ Å, $\kappa = 50\ \mathrm{N\,m^{-1}}$, $\Phi = 2500$ pN. B) Force–distance curves according to the WLC model. The chain can be more easily stretched (lower restoring force at the same extension) by increasing the persistence length. The tendency for coiling is reduced and, thus, it becomes easier to stretch the polymer to form a linear chain. However, it is noteworthy, that the WLC polymer cannot be stretched beyond its contour length.

Table 4. Mechanical parameters of different molecules according to the FJC model (FJC$^+$).

Polymer	Kuhn length [Å]	Segment elasticity [N m^{-1}]
polystyrene[128] in toluene	12.2	2.1
polyvinyl alcohol[129] in aqueous solution	6.2	17
polyethyleneglycol[100] in hexadecane	7	150
P-selectin/PSGL-1[127] in aqueous solution	7 ± 1	0.8 ± 0.2

The following approximation gives an expression for the force–distance relationship[132] [Equation (15)],[105, 133] which

$$F(x) = \frac{(k_B T)^2}{B}\left[\frac{1}{4}\left(1-\frac{x}{L}\right)^{-2}+\frac{x}{L}-\frac{1}{4}\right] = \frac{k_B T}{l_P}\left[\frac{1}{4}\left(1-\frac{x}{L}\right)^{-2}+\frac{x}{L}-\frac{1}{4}\right] \quad (15)$$

is accurate up to several 100 pN. The persistence length, like the Kuhn length, represents the flexibility of the molecule. B denotes the bending module of the polymer.[134] The chain direction is preserved on the length scale of the persistence length, and below the persistence length the polymer can be considered to be linear.[135] In other words: molecules with high persistence length have a tendency *not* to form coils. Strictly speaking, the persistence length is a function of the external force.[109, 136–138] This fact explains why recombinant titin fragments exhibit a persistence length of 8 Å at low forces, whereas the molecule shows a persistence length of merely 4 Å at forces higher than 50 pN (see Table 7). The WLC model has been successfully applied to describe the elastic behavior of DNA, poly(methacrylic acid), muscle, and adhesion proteins (Table 5). For very small extensions ($x \ll L$)

Table 5. Mechanical parameters of different molecules according to the WLC model.

Polymer	Persistence length [Å]
polydimethylsiloxane[126] in heptane	2.3 ± 0.2
polymethacrylic acid[116] in aqueous solution	2.8 ± 0.5
proteoglycane[30] in aqueous solution	4.8

the difference between the WLC and the FJC model is negligible, since the equilibrium conformation of the molecule is Gaussian-like. At low forces, the persistence and Kuhn length are related by: $l_K = 2l_P$.[139]

It needs to be emphasized that the discussed models are independent of the molecular composition of the polymer. The WLC model assumes a continuum without fine structure. Usually, no simple relation between the model parameters l_P and l_K and real structural quantities such as bond length or the length of a monomer unit can be found: for DNA, l_P is approximately 500 Å and thus considerably larger than the helical pitch of the duplex (34 Å) or the diameter of the helix (25 Å). In the case of dextran, however, the Kuhn length (ca. 4.4 Å) and the length of a monomer (ca. 5 Å) are rather close.[110] The structure of a polymer depends on the environment and hence, also on the Kuhn and persistence length. The approach, which is most suited to describing the experimental data, depends on the polymer and the force regime.

5.2.5. The Extended WLC Model: Enthalpic Stretching

Although the standard WLC model already includes bending elasticity, the extended WLC model includes the stiffness of the chain [Eq. (16)].The parameter Φ denotes the specific stiffness of the polymer.[140] Equation (16) describes the elastic properties of DNA at elevated forces more realistically than the classic WLC model.[141]

$$F(x) = \frac{k_B T}{l_P}\left[\frac{1}{4}\left(1-\frac{x}{L}+\frac{F}{\Phi}\right)^{-2}+\frac{x}{L}-\frac{F}{\Phi}-\frac{1}{4}\right] \quad (16)$$

5.2.6. Modular Polymers: A Two-State Model

Force-induced conformational changes are often accompanied by a lengthening of the molecule backbone. A spontaneous structural change is extremely improbable since it is energetically unfavorable. Without the presence of an external force, the polymer is in the ground state. An external force, however, can give rise to a repeated unfolding of protein domains as shown for spectrin, titin, and tenascin. The subunits of the modular proteins change from a folded (length l_1) to an unfolded, extended state (length l_2).

Following the FJC model, the number of subunits n is constant during extension but every subunit has two possible

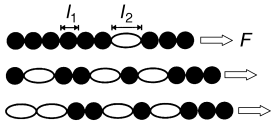

Figure 16. Part of a polymer chain whose subunits may show two different length states (l_1 and l_2). An external force F favors the transition of the coiled state 1 to the stretched state 2. This conformational change occurs randomly along the chain.

states 1 and 2, which are independent of each other (Figure 16): $n = n_1(F) + n_2(F)$.[106] Hence, the contour length becomes a function of the external force: $L(F) = n_1(F)\, l_1 + n_2(F)\, l_2$. If the force–extension curves are reversible, that is, the trace and retrace are identical, the system is in equilibrium. Structural changes are fast relative to the timescale of the experiments, which is usually in the range of seconds. The final state—thermal equilibrium—is reached instantaneously. Therefore, the distribution of the states can be expressed in terms of a Boltzman distribution: $n_2/n_1 = \exp(-\Delta G(F)/k_B T)$. The free enthalpy ΔG depends on the external force, which causes a continuous reduction in the energy barrier of the conformational transition $\Delta G(F) = (E_2 - E_1) + F(l_2 - l_1)$. In the case of the extended FJC model [Eq. (14)] this leads to expression (17). Again the relevant length scale is the contour length of the polymer: $n = L/l_K$ at $F = 0$.

$$x(F) = L(F)\mathbf{L}\left(\frac{F\,l_K}{k_B T}\right)\left(1+\frac{F}{\kappa L}\right) \qquad (17)$$
$$= \frac{L}{l_K}\left(\frac{l_1}{\exp(-\Delta G(F)/k_B T)+1} + \frac{l_2}{\exp(+\Delta G(F)/k_B T)+1}\right)\mathbf{L}\left(\frac{F\,l_K}{k_B T}\right)\left(1+\frac{F}{\kappa_L}\right)$$

Figure 17 shows the applicability of the theory by stretching polyethyleneglycol in aqueous solution until an irreversible structural change occurs.[100] The energy barrier between the all-*trans*-(ttt) state and the ttg conformation of the monomers

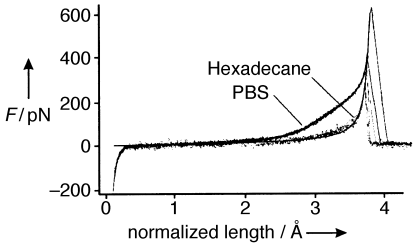

Figure 17. A number of normalized force curves are displayed (pulling forces are positive) for single polyethyleneglycol molecules (PEG) dissolved in hexadecane or PBS buffer and functionalized by a thiol or butoxy group on a gold substrate. Along the abscissa, the relative displacement is plotted multiplied by the monomer length. In an aqueous environment PEG adopts a helical conformation, which turns into a stretched state upon exerting an external force at one end. The stretching behavior at low forces can be well described with the modular FJC$^+$ model [Eq. (17)]. However, in an organic solvent (hexadecane) formation of intermolecular hydrogen bonds which stabilize the helical conformation is abolished. In this case, the enthalpic FJC model is appropriate.[100]

was determined to be $E_2 - E_1 = (3.0 \pm 0.3)\, k_B T$. However, hydrogen bonds are missing in organic solvents such as hexadecane and the PEG filaments can no longer be described by the enthalpic FJC model. The value of the energy barrier was predicted by quantum mechanics calculations. In a very similar approach it is feasible to analyze the folding of proteins quantitatively using the WLC model.

In many cases the stretching of molecules is irreversible as evident from the hysteresis between the approach and retraction curve. If the potential is asymmetric, that is, the potential width of unfolding is small relative to that of refolding, very different rate constants for folding and unfolding result. It was shown that in the case of titin, a muscle protein, refolding is very unlikely, thus the stretching of titin is an irreversible process. While the width of the potential for unfolding x_u is small (0.3 nm), the one for folding x_f is rather large (15 nm).[109] If an external force is applied the rate of refolding is decreased as shown in Figure 18A. Therefore, the unfolding force depends on the pulling velocity. Small pulling velocities result in small unfolding forces. This observation is analogous to the results obtained from experiments on the force-induced rupture of ligand–receptor couples.

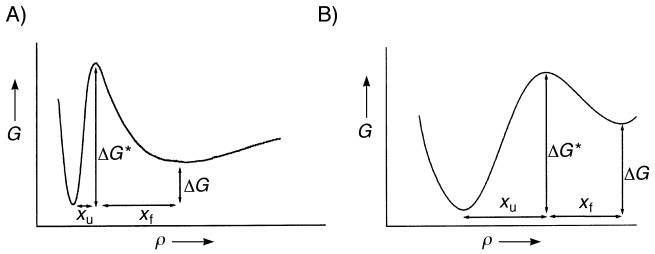

Figure 18. Schematic drawing of the two-state model of the unfolding of polymers. A) An asymmetric potential results in an irreversible unfolding/stretching of the polymer (for example, titin) at the timescale of the experiment. B) A symmetric potential with narrow potential widths, such as in the case of dextran filaments, however, causes a reversible conformational change during expansion and compression cycles.

5.2.7. A Criterion for Single-Molecule Detection

Interpretation of force–distance curves can be difficult. It is seldom the case that only single molecules are located between the tip and the sample. Usually many filaments are stretched quasi-simultaneously and detach from either the sample or the tip shortly after the other. How can we decide whether an individual molecule or a bundle of several filaments has been extended?

All the models have one thing in common: $F(x)$ is a function of x/L. It seems reasonable that the elasticity of a linear polymer scales with its contour length. Longer polymers are softer than shorter ones. Two polymer filaments of different length exhibit different extension curves. The intrinsic properties, however, such as l_K, κ, Φ, and l_P are independent of the polymer length. Thus, polymers of the same molecule but different length can be described by a common force–extension curve $F(x/L)$. Figure 19 displays the force F versus the normalized displacement x/L. This graph enables one to compare force–distance curves of different filaments. The agreement between normalized curves is strong evidence for single molecules.

This approach requires the determination of the contour length L for every single filament, that is, one has to fit the parameters of the corresponding polymer model to the data. But there is an easier way to normalize force–distance curves: a given force–extension curve of filament "a", $F_a(x)$, has to be transformed into $F_a(x/x_a^*)$ under the condition:

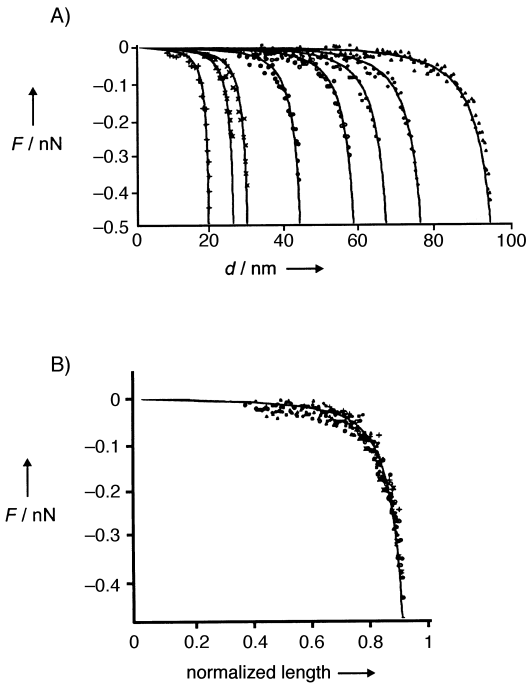

Figure 19. A) Force–distance curves of polymethacrylate filaments of different contour lengths together with curve fits according to the WLC model. B) By normalizing the force curves it becomes clear that single molecules of one class are indeed observed. Loss of contact occurs if the molecules are stretched to 90% of the contour length.[116]

$F_a(x_a^*) = F^*$. In principle, the force F^* can be chosen arbitrarily. However, it is wise to choose a rather large value for F^* (if there is one) in the range of a conformational transition. From the experimental data x_a^* merely needs to be determined. This method can be applied to filament "b", in which the force F^* is the same for all filaments ($F^* = F_a(x_a^*) = F_b(x_b^*) = \ldots$). If all normalized curves coincide ($F_a(x/x_a^*)$, $F_b(x/x_b^*)$, ..), all the filaments belong to the same class. The filaments are then either supramolecular structures or single polymer molecules. That means that normalizing the data is independent of the polymer model, with the only requirement that the force needs to be dependent on the displacement x/L.[142]

The determination of molecular forces on the level of single molecules is accompanied by several difficulties. Besides problems concerned with instrumentation, such as the determination of spring constants and limited pulling velocities, the surface chemistry can play a pivotal role if controversial results are obtained. In some cases different binding strengths for the same complex were obtained dependent on the surface chemistry. Background adhesion and different tip radii can influence the data. Particularly, the determination of the binding strength of DNA has apparently led to controversial results. Contaminations might be a problem if elastic properties of filaments are described.

5.3 Polysaccharides

The mechanical properties of many polysaccharides can be described by the extended FJC model. A summary of the experimental data obtained from different types of polysaccharides is given in Table 6.

Experiments with dextran, which is composed of $\alpha 1 \rightarrow 6$-linked glucose monomers, demonstrate that force spectroscopy gives valuable information about the molecular mechanics of filamentous molecules. The occurence of a shoulder in the force–extension curve for the extension of dextran is typical.[45] The shoulder arises from a reversible structural change accompanied by a stiffening of the molecule. Amylose, a polysaccharide consisting of $\alpha 1 \rightarrow 4$-connected pyranose monomers, exhibits a similar behavior. The force–extension curve below the conformational change can be described by means of the extended FJC model (Table 6). Monte Carlo simulations match with the observed force–extension curves and reveal the equilibrium constant K and in turn the energy barrier for the conformational transition: $E_2 - E_1 = 13.2\, k_B T = k_B T \ln K$.[109]

Table 6. Molecular parameters of different polysaccarides in aqueous solution. $E_2 - E_1$: energy barrier of two conformations; Δx_u, Δx_f: potential width, v: pulling velocity.

Polymer	Kuhn length [Å]	Transition at F^* ($v \approx 1\ \mu m\, s^{-1}$)	Segment elasticity [$N\, m^{-1}$]
dextran[45, 109] (native)	–	700–850 pN (reversible) $E_2 - E_1 = 13.2\, k_B T$ (C_5–C_6 flip) $\Delta x_u = \Delta x_f = 0.32$ Å	8 ± 1 ($F < F^*$) 40 ± 10 ($F > F^*$)
dextran[110] (native)	4.4 ($F < F^*$) 5.7 ($F > F^*$)	850 ± 140 pN (reversible) $E_2 - E_1 = 18.6\, k_B T$ (chair→boat) $\Delta x_u + \Delta x_f = 1.284$ Å	14.6 ± 2.7 ($F < F^*$)
dextran[45] (carboxymethylated)	6 ± 0.5 ($F < F^*$)	250–350 pN (reversible)	6.7 ($F < F^*$) 17 ($F > F^*$)
dextran[110] (periodate oxidation)	2 ± 0.26	–	34.2 ± 8.3
amylose[110, 152] (native)	4.5 ($F < F^*$) 5.4 ($F > F^*$)	275 ± 45 pN (reversible) E_2-$E_1 = 7.7\, k_B T$ (chair→boat) $\Delta x_u + \Delta x_f = 0.44$ Å	5.6 ± 0.8 ($F < F^*$)
amylose[110] (periodate oxidation)	1.8 ± 0.25	–	34 ± 7.3
pullulan[110] (native)	4.5	–	10.2 ± 0.93
Pullulan[110] (periodate oxidation)	2 ± 0.15	–	47.8 ± 5
xanthan[99] (native)	–	400 pN (irreversible)	
xanthan[99] (denaturated)	–	–	5 ± 0.5
cellulose[99] (carboxymetylated.)	–	–	5 ± 0.5

But what happens during the conformational change on the molecular level? Molecular dynamics simulations indicate that deformation of the O-glycosidic bond occurs. Every glucose monomer experiences a lengthening of 0.6 Å, that is by about 10%. This would explain the plateau of the force–extension curve (Figure 20). The deformation of the bond is fully reversible: the bond angles snap back to their original position upon relaxation.

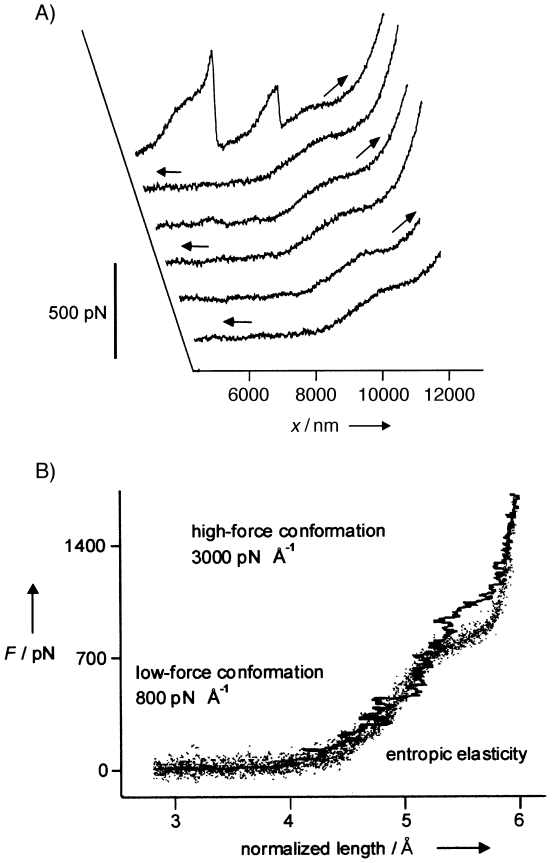

Figure 20. A) Subsequent force measurements of carboxymethylated dextran. In the first curve two short-chain molecules are torn apart. The remaining molecule can be stretched and relaxed several times without loss of contact. The characteristic "shoulder" observed at a force of approximately 300 pN results from a conformational transition of the polysaccharide chain. Curves that are monitored one after the other coincide. This result demonstrates that the structural change occurs in thermodynamic equilibrium (pulling velocity was ca. 1 $\mu m s^{-1}$). B) In a normalized presentation the single molecule character of the native dextran molecules can be observed readily; all curves show the same course (x/L was multiplied by the length of one dextran molecule). The structural transition occurs at approximately 700 pN. The dark curve is the result of molecular dynamic simulations.[6, 45, 110]

Two different conformational changes of the pyranose monomer are conceivable, the *trans-gauche* transition of the O-glycosidic bond of the $\alpha 1 \rightarrow 6$-glycosidic dextran and a chair–twisted-boat transition of amylose with $\alpha 1 \rightarrow 4$-glycosidic bonds.[143] Both changes account for the stretching of the filament. Ab-initio calculations reveal that the external force can cause a transition from the chair to the energetically unfavorable twisted-boat conformation. The energy barrier is: $E_2 - E_1 = 18.6 k_B T$.[110] This value is comparable to the result obtained from Monte Carlo simulations (see above).

The oxidation of pyranose with periodate abolishes the conformational transition and the shoulder in the force–extension curve vanishes.[110] Dextran, amylose, and pullulan display almost the same behavior upon extension (Table 6). The opening of the sugar ring elicits a stiffening of the polysaccharides, which emphasizes the influence of the ring structure on the mechanical properties of the material.

An example of a polysaccharide exhibiting an irreversible conformational change is xanthan[99] (Figure 21). In its native state xanthan exhibits a helical conformation that is stabilized

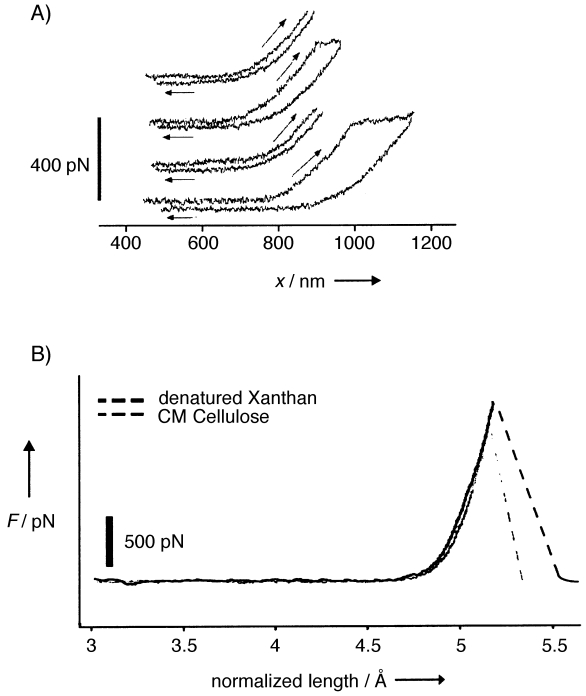

Figure 21. A) Several force–distance curves of native xanthan directly monitored one after the other without loss of the molecular contact.[99] The extension of the polymer was subsequently increased until a plateau occurred at a force of approximately 400 pN. A hysteresis between the back and forward direction was observed; on the timescale of the experiment, the conformational transition occurs in a thermodynamic nonequilibrium. B) Denatured xanthan and carboxymethyl cellulose exhibit practically identical features. The normalized distance is multiplied by the length of a glucose monomer.[99]

by noncovalent interactions. The unfolding of the secondary structure is accomplished by applying an external force. Denatured xanthan, which exhibits no helical conformation, shows no conformational transition within the force–extension curve.[99] The mechanical properties of denatured xanthan resembles those of carboxymethylcellulose, which has the same $\beta 1 \rightarrow 4$-Glc-backbone.[99]

5.4. Polynucleotides

The mechanical properties of DNA are of great interest as a consequence of its biological significance. Its elasticity has been extensively studied by means of optical tweezers—the molecule is trapped by a laser beam—and other methods of micromanipulation.[144] The number of investigations per-

formed with the force microscope is also increasing.[24, 85, 87] The advantage of force spectroscopy over optical tweezers is the possibility of exerting forces in the nanonewton range. Most studies with common techniques are limited to forces below 100 pN. Remarkable structural changes already occur in this range, however.[85, 86, 88, 89, 108] This section provides a survey dealing with the mechanics of DNA as probed by the scanning force microscope.

The mechanical properties of DNA are not only of academic interest. In the active cell the active gene must become accessible in order for replication, regulation, and transcription to occur, although DNA is packaged by proteins. Force spectroscopy measurements on polyinosine revealed that single-stranded DNA (ssDNA) behaves like an entropic (extensible) chain.

The elastic properties of double-stranded DNA (dsDNA), however, are more complex. A comprehensive review on the mechanical properties of DNA is given by Austin et al.[102] As a consequence of its double-helix structure dsDNA is very stiff and less flexible than ssDNA. Many experiments employ λ-phage DNA. Conformational changes and smaller forces occur at smaller forces than in polysaccharides (Section 5.3), which makes a sensitive method of detection necessary.

Below 60 pN the extended WLC model is most suited for describing the mechanical behavior of dsDNA. However, exerting higher forces results in significant structural changes. Native dsDNA adopts the so-called *B* conformation and changes to the *S* conformation (S: stretched) at 65 pN. The transition occurs fast within a force range of approximately 5 pN, which is indicative of a process of high cooperativity. At this point, the molecule can be stretched to almost twice its contour length (Figure 22).[85] Notably, before the structure of DNA was unraveled, there were speculations in the fifties about these kind of elastic properties.

The transition from the *B* to the *S* conformation is probably accompanied by a decoiling of DNA. Léger et al. showed that the force where the $B-S$ transition occurs depends on the number of twists. Different DNA structures were characterized in this way.[145] The opened *S*-DNA conformation facilitates access to the base pairs compared to the *B* conformation. This situation might be relevant for DNA transcription. The structure and reason for the high cooperativity remain to be elucidated. Molecular dynamics simulations indicate that two different structures are conceivable in the stretched conformation.[146] It is difficult to distinguish between them on the basis of force measurements since the deformation energies for both structures are almost identical. It is important for the reaction pathway on which strand the force is exerted and whether the molecule can rotate freely during extension. In the case of free rotation, the helix can be entirely uncoiled. However, if rotation is suppressed the direction of the base pairs changes. Pulling causes a bending of the base pairs with respect to the longitudinal axis, which is accompanied by a reduction in the diameter of the helix. There are some indications that the flat ribbonlike structure of DNA has some significance under physiological conditions. It is conceivable that this conformation is stabilized by DNA-binding proteins.

The melting of the DNA occurs at higher forces of around 150 pN. Both the melting of DNA and the *B* to *S* transition at low forces are sequence dependent. Duplex-poly(dA-dT)- and duplex-poly(dG-dC)-DNA exhibit a self-complementary base sequence, which can result in the formation of hairpin loops after relaxation. Rief et al. studied the reversibility of melting and the conformational change of the *B* to the *S* form.[85] They found that the $B-S$ transition occurs much faster than the withdrawal of the cantilever (the pulling velocity is in the range of $\mu m\,s^{-1}$) and is therefore fully reversible. Moreover, the threshold force is not dependent on the pulling velocity either. The melting of DNA, however, depends on the pulling velocity and displays a typical hysteresis between the approach and retraction curves, which indicates an irreversible process.

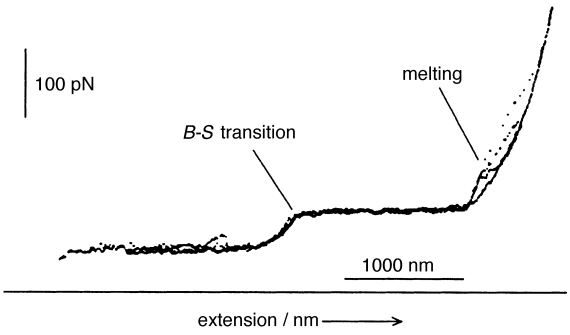

Figure 22. Superposition of different force–extension curves of dsDNA from the λ-phage obtained at different pulling velocities ($0.15-3\ \mu m\,s^{-1}$). The contour length of the molecule is approximately 2 μm. A conformational change from the *B* to the *S* conformation occurs at 65 pN. At this point the DNA can be stretched beyond 3 μm without any detectable increase in the restoring force. The nucleotide strands separate (melt) at approximately 150 pN. The force at which this event takes place depends on the pulling velocity. The process is therefore irreversible. Despite the partial melting of dsDNA (hysteresis) the *B* state is formed upon relaxation. This can be deduced from the overlap of the back and forward *z* scan immediately before the $B-S$ transition occurs. Even after reaching the actual melting transition this can occur, however, it is not inevitable.[85]

5.5. Polypeptides and Proteins

Many proteins are designed to cope with mechanical load: actin and myosin[147] are responsible for muscle contraction, whereas the stability of connective tissue and cartilage are based on extracellular matrix proteins such as laminin, collagen, vimentin, fibronectin, and proteoglycans.[148] Individual cells may migrate on surfaces because of elastic anchor proteins. Leukocytes are known to roll along the endothelium of blood vessels if pushed ahead by the bloodstream. The contact between endothelial cells and the white corpuscles is established by proteins, which are stretched during rolling. The elasticity of these molecules is based on their particular structure and intramolecular interactions—mostly noncovalent interactions and disulfide bridges. Besides hydrogen bonding, electrostatic interactions and hydrophobic effects are responsible for the stability of proteins. It has not been possible to distinguish between the different kinds of interactions by force spectroscopy. However, collective forces that determine the shape of the protein domains can be measured accurately.

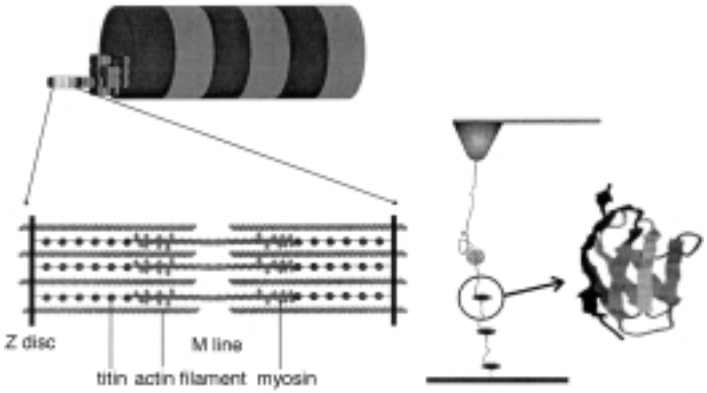

Figure 23. Titin, the most well-known elastic filament, stems from the sarcomer of striped muscles and is responsible for elastic anchoring and central orientation of the myosin filaments. Titin is a 3000 kDa protein and is one of the largest proteins known. It is composed of tandem fibronectin III (FN3) and structurally related immunoglobulin (Ig) domains (constant region). FN3 domains are composed of 98 – 102 amino acids and possess seven β-sheet peptide chains that form a β-barrel. Ig domains exhibit essentially the same structure. The elastic stretching of the I band, which can be four times larger than the original length, can only be explained by a reversible folding and unfolding of the FN3 and Ig domains.

Until now, linear muscle and adhesion proteins, such as titin (Figure 23) and tenascin, which consist of globular subunits have been preferred for investigation. Stretching such a modular protein results in the subsequent unfolding of the globular domains: the sequence is determined by the stability of the subunits: the less-stable units unfold before the more-stable ones. Each unfolding event is accompanied by a sudden lengthening of the filament (Figure 24 B). The unfolding of a single domain results in a fast relaxation of the bent cantilever. This process is repeated for each subunit upon extension of the filament and results in a saw-tooth profile of the force – extension curve (Figure 24 A). Such a curve was observed for native and recombinant proteins such as titin, tenascin, and spectrin.

The change from the folded to the unfolded state of each domain is highly cooperative without the occurrence of intermediate species. Therefore, the process can be described by means of a two-state model, which has turned out to be useful in interpreting the rupture of ligand – receptor couples (Figure 18) or the force – induced conformational changes of dextran (Figure 20). The mechanism is always identical: Pulling the cantilever reduces the energy barrier separating the folded and unfolded states until thermal fluctuations bring about the structural change. The refolding of a molecule such as titin is unlikely because of the high asymmetry of the potential $x_f \ll x_u$. The folding rate is negligibly small under external force. The stretched polypeptide chain has to contract itself against the external force over a length of more than 100 Å. Therefore, the conformational change does not occur in thermal equilibrium. This change is in contrast to the conformational change of dextran, which displays only an extension of 0.32 Å at pulling velocities of a few $\mu m\,s^{-1}$, and is therefore fully thermodynamically reversible. The measurement of forces of systems that are not performed in thermal equilibrium have the following consequences:

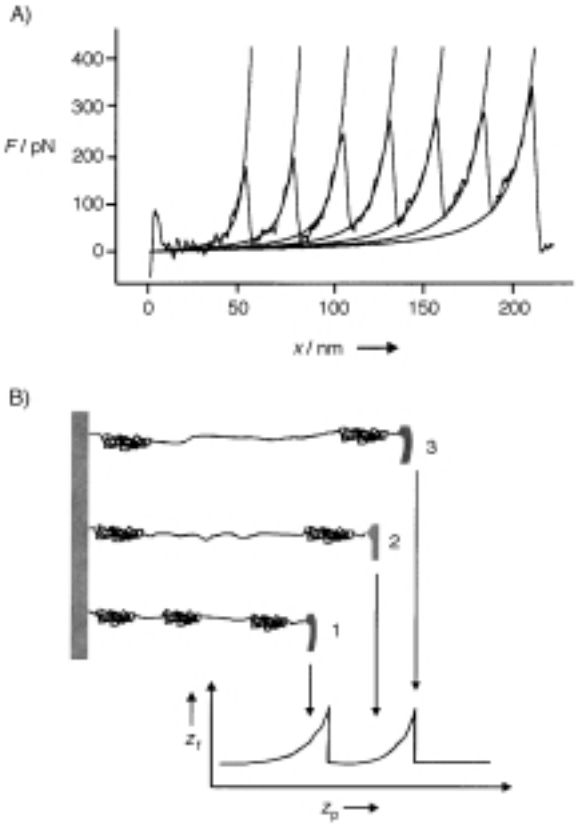

Figure 24. A) Force-induced conformational change of a recombinant titin fragment. Seven immunoglobulin domains unfold subsequently without removal of the molecule from the tip or detachment of the molecules from the substrate. The partial curves can be described by the WLC model (l_P = 4 Å) in which the contour length increases each time by 280 Å.[152] B) Schematic representation of the ascribed process. The polypeptide strand that is folded in several domains is unfolded one domain after the other, with the weakest domains unfolding first: the tip takes up the molecule and stretches it (1). If the domain unfolds (2) the tip – sample distance suddenly increases. The free polypeptide strand is stretched (2 – 3) until the pulling force reaches a threshold value and the domain unfolds.[152]

1) The refolding of a stretched molecule is slow compared to the timescale of the experiment. Since equilibrium does not occur immediately, the kinetics of the reaction has to be considered. Thus, the force at which unfolding occurs depends on the pulling velocity (Figure 25 A).

2) The force – extension curve is characterized by a hysteresis of the approach and retraction curve since the structural change of the molecule is irreversible within the timescale of the experiment (Figure 25 B).

Cross-linked polylysine at pH 7 exhibits a reversible extension (Figure 26).[68] It was possible to extend and stretch the molecule within one minute without any detectable changes in the force – extension curve. At the end of force curve 72 an irreversible overstretching occurred and resulted in a smaller persistence length. Computer simulations of the reaction kinetics provide information about parameters (Table 7) such as the potential width of the conformational transition and the unfolding rate. If, however, the transition occurs within thermal equilibrium, as is the case for dextran, the rate constants cannot be determined separately.

Since force spectroscopy is capable of detecting small variations in the number of amino acids, it is possible

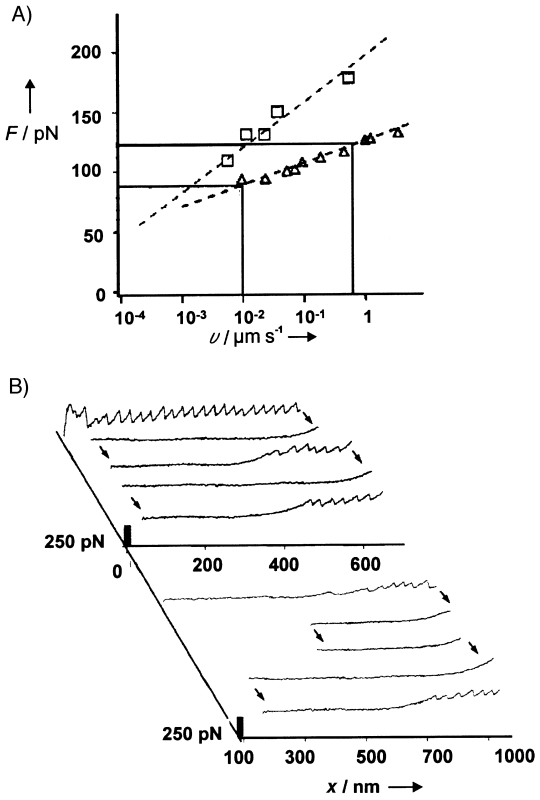

Figure 25. A) Unfolding force as a function of pulling velocity (semi-logarithmic plot). Values for native titin (□) and tenascin–fibronectin (△), a recombinant fragment of similar structure, are shown. The dashed lines are the results of computer simulations.[136] B) The subsequent force measurements of titin reveal a hysteresis; on the timescale of the experiment the conformational transition is irreversible. Since the refolding of the molecule is very slow, the first stretching curve exhibits more unfolding events than the following ones. Only when the time between the extension and relaxation were longer could the saw-tooth profile be fully regained. The applied force prevents refolding of the genuine molecular structure. Only when the protein is relaxed can the saw-tooth pattern be observed again.[152]

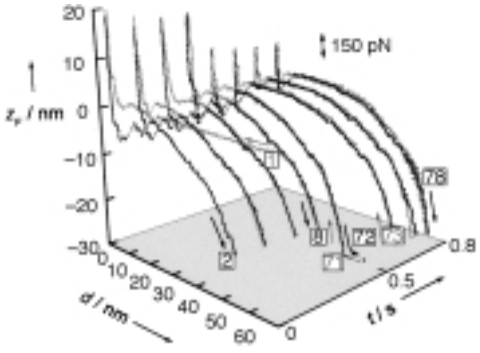

Figure 26. Reversible unfolding–folding cycles of poylysine (gold-covered Si_3N_4 tip acts on a gold substrate covered with thiolated poly-L-lysine (pH 7, pulling velocity 100 nm s^{-1}). The numbers indicate the sequence of measurements. The overstretching of the molecules after 72 force–distance curves results in a decrease in the chain stiffness. Polylysine was derivatized using iminothiolane in order to ensure attachment of the molecules on the gold.[68]

to explore basic differences in the primary structure of the protein. This can be demonstrated by a comparison between spectrin and titin. Spectrin consists of α-helix bundles, while titin subunits exhibit a β-barrel structure. Both molecules denature at almost the same temperature; thus, the activation energy of unfolding is also similar. However, the forces which are necessary to unfold spectrin are much lower than those needed to unfold titin. The reason for this can be found in the course of the folding–unfolding potential. Although the height of the energy barrier of spectrin is similar to that of titin its width is six times larger (Table 7). Consequently, the unfolding state is very shallow and more extended than that of titin, that is, the measured unfolding forces of spectrin domains are lower by nearly the same factor.

Table 7. Molecular parameters of different proteins in aqueous solution. Immunoglobulins (Ig), the repeating units of titin, and fibronectin-III domains (Fn-III), subunits of tenascin and titin, have a similar structure (β-barrel). Spectrin, however, consists of α-helical subunits. Spectrin stabilizes the cytoskeleton of erythrocytes. Tenascin originates from the extracellular matrix, while titin is found in muscles. Only few data are available from the nonlinear α_2-macroglobulin. α_u, α_f [s]: unfolding and folding rate, respectively, in the absence of an external force, Δx_u, Δx_f [Å]: width of the energy barrier of unfolding and folding, respectively, v: pulling velocity.

Polypeptide	Persistence length [Å]	Transition (domain folding) $v = 0.01 - 0.5$ μm s^{-1}	Lengthening [Å]
Ig peptide[137, 138, 152] (recombinant titin fragment), titin[109, 152] (native)	8 (<50 pN) 4 (>50 pN)	130 pN/190 pN $\alpha_u = 0.3 \times 10^{-4}$ $\alpha_f = 2$ $\Delta x_u = 3$ $\Delta x_f > 150$	266 280
Fn-III peptide[153] (recombinant tenascin fragment), tenascin[153] (native)	4.2 ± 2.2 (>50 pN)	~90 pN/~150 pN $\alpha_u = 4.6 \times 10^{-4}$ $\alpha_f = 3$ $\Delta x_u = 3$, $\Delta x_f = 10$	285 ± 40
Fn-III peptide[137] (recombinant tenascin fragment)	8 (<50 pN) 4 (>50 pN)	ca. 90 pN/~160 pN $\alpha_u = 0.3 \times 10^{-4}$ ($l_P = 4$ Å) $\Delta x_u = 5.5$	286
spectrin[138] (native)	8 (<50 pN)	<25 pN/ca. 30 pN $\alpha_u = 0.3 \times 10^{-4}$ $\Delta x_u = 17 \pm 5$	317 ± 3
α_2-macroglobulin[29]	stiffness: ca. 15 mN m^{-1}, ca. 65 mN m^{-1}		

In contrast to the β-barrel structures, the tertiary structure of spectrin is not stabilized by hydrogen bonds. Hydrogen bonds only stabilize the helix itself, and not the entire bundle. Thus, the tertiary structure is mainly maintained by weak hydrophobic interactions that lead to smaller unfolding forces. It remains to be elucidated whether the different mechanical stabilities of the two proteins are of any biological significance.

6. Summary and Outlook

Wo rohe Kräfte sinnlos walten,
da kann sich kein Gebild gestalten."

Friedrich von Schiller (1759–1805), *Lied von der Glocke*

With regard to force measurements this quotation from the German dramatist Schiller should read instead: "Wo rohe Kräfte sinnlos walten, da kann sich kein Gebilde *falten*." since high forces and pulling velocities can rupture bonds and unfold proteins but render binding and folding highly improbable. The simple model of Bell[80] can describe most

of the results obtained from force measurements. It should be emphasized that reversible conformational changes are not excluded, but depend on the topology of the potential and the pulling velocity of the cantilever. Examples of a reversible transition between two conformations upon exerting an external force are the change from the chair to the twisted-boat conformation of dextran as well as the change from the *B* to *S* conformation of the DNA duplex. Irreversible processes are characterized by a hysteresis between the approach and retraction of the cantilever, a dependence of the force at which the transition occurs on the pulling velocity, and an asymmetric potential. For example, the extension of modular proteins such as titin, a filamentous muscle protein, spectrin from erythrocytes, and tenascin, an extracellular protein, shows that kinetic analysis according to a classic two-state model in conjunction with generic polymer models permits qualitative as well as quantitative data to be derived on the mechanical properties of polymers.

Force microscopy has developed into a powerful tool for probing the mechanical properties of single molecules such as conformational transition states, bending modules, binding strength, rate constants, and the topology of the potential. Future prospects have been intimated by Müller, who reported the first experiments on the folding and unfolding cycles of bacteriorhodopsin in its native environment in conjunction with high resolution imaging.[149] It was shown that single helices could be removed from the bundle assembly. Besides experiments with isolated systems, the first force experiments with whole cells have been conducted on the quantification of cell adhesion.[150]

Scanning force spectroscopy combines high-resolution imaging with manipulation of single molecules and provides the possibility of obtaining insights into the mechanical behavior and structural details of synthetic polymers and biomolecules on a molecular level.

We would like to thank Bernd Gotsmann and Claudia Steinem for the critical reading of the manuscript and many fruitful discussions.

Received: December 6, 1999 [A 373]

[1] J. N. Israelachvili, D. Tabor, *Proc. R. Soc. London A* **1972**, *331*, 19.
[2] G. Binnig, C. F. Quate, C. Gerber, *Phys. Rev. Lett.* **1986**, *56*, 930.
[3] a) D. Krüger, B. Anczykowski, H. Fuchs, *Ann. Phys.* **1997**, *6*, 341; b) B. Anczykowski, B. Gotsmann, J. P. Cleveland, H. Fuchs, V. B. Elings, *Appl. Surf. Sci.* **1999**, *140*, 376; c) B. Gotsmann, C. Seidel, B. Anczykowski, H. Fuchs, *Phys. Rev. B* **1999**, *60*, 11051; d) B. Gotsmann, C. Schmidt, C. Seidel, H. Fuchs, *Eur. Phys. J. B* **1998**, *4*, 267.
[4] E.-L. Florin, V. T. Moy, H. E. Gaub, *Science* **1994**, *264*, 415.
[5] G. U. Lee, D. A. Kidwell, R. J. Colton, *Langmuir* **1994**, *10*, 354.
[6] "Kraftspektroskopie an einzelnen Molekülen": M. Rief, Dissertation, Munich, **1997**.
[7] H. Heinzelmann, E. Meier, H. Rudin, H.-J. Güntherodt, *Force Microscopy in scanning tunneling microscopy and related methods* (Ed.: R. J. Behm), Kluwer-Academic, Amsterdam, **1990**.
[8] M. Radmacher, R. W. Tillman, M. Fritz, H. E. Gaub, *Science* **1992**, *257*, 1900.
[9] H. G. Hansma, J. H. Hoh, *Annu. Rev. Biophys. Biomol. Struct.* **1994**, *23*, 115.
[10] B. Capella, P. Baschieri, C. Frediani, P. Miccoli, C. Ascoli, *IEE Eng. Med. Bio.* **1997**, March/April, 58.
[11] J. H. Hoh, J. P. Cleveland, C. B. Prater, J.-P. Revel, P. K. Hansma, *J. Am. Chem. Soc.* **1992**, *114*, 4917.
[12] R. Ros, F. Schwesinger, D. Anselmetti, M. Kubon, R. Schäfer, A. Plückthun, L. Tiefenauer, *Proc. Natl. Acad. Sci. USA* **1998**, *95*, 7402.
[13] C. D. Frisbie, L. F. Rozsnyai, A. Noy, M. S. Wrighton, C. M. Lieber, *Science* **1994**, *265*, 2071.
[14] S. Akari, D. Horn, H. Keller, W. Schrepp, *Adv. Mater.* **1995**, *7*, 549.
[15] C. E. H. Berger, K. O. van der Werf, R. P. H. Kooyman, B. G. de Grooth, J. Greve, *Langmuir* **1995**, *11*, 4128.
[16] J. L. Wilbur, H. A. Biebuck, J. C. MacDonald, G. M. Whitesides, *Langmuir* **1995**, *11*, 825.
[17] M. Ludwig, W. Dettmann, H. E. Gaub, *Biophys. J.* **1997**, *72*, 445.
[18] G. Bar, S. Rubin, A. N. Parikh, B. I. Swanson, T. A. Zawodzinski, Jr., M.-H. Whangbo, *Langmuir* **1997**, *13*, 373.
[19] E. W. van der Vegte, G. Hadziiannou, *J. Phys. Chem.* **1997**, *101*, 9563.
[20] J. N. Israelachvili, *Intermolecular and Surface Forces*, 2nd ed., Academic Press, London, **1991**.
[21] H.-J. Butt, *Biophys. J.* **1991**, *60*, 777.
[22] W. A. Ducker, T. J. Senden, R. M. Pashley, *Nature* **1991**, *353*, 239.
[23] A. Marti, G. Hähner, N. D. Spencer, *Langmuir* **1995**, *11*, 4632.
[24] G. U. Lee, L. A. Chrisey, R. J. Colton, *Science* **1994**, *266*, 771.
[25] T. Boland, B. D. Ratner, *Proc. Natl. Acad. Sci. USA* **1995**, *92*, 5297.
[26] L. A. Wenzler, G. L. Moyes, L. G. Olson, J. M. Harris, T. P. Beebe, Jr., *Anal. Chem.* **1997**, 69, 2855.
[27] P. Hinterdorfer, W. Baumgartner, H. J. Gruber, K. Schilcher, H. Schindler, *Proc. Natl. Acad. Sci. USA* **1996**, *93*, 3477.
[28] L. A. Wenzler, G. L. Moyes, G. N. Raikar, R. L. Hansen, J. M. Harris, T. P. Beebe, Jr., *Langmuir* **1997**, *13*, 3761.
[29] K. Mitsui, M. Hara, A. Ikai, *FEBS Lett.* **1996**, *385*, 29.
[30] J. Fritz, D. Anselmetti, J. Jarchow, X. Fernandez-Busquets, *J. Struct. Biol.* **1997**, *119*, 165.
[31] M. Heuberger, G. Dietler, L. Schlapbach, *J. Vac. Sci. Technol. B.* **1996**, *14*, 1250.
[32] A. Vinckier, P. Gervasoni, F. Zaugg, U. Ziegler, P. Lindner, P. Groscurth, A. Plückthun, G. Semenza, *Biophys. J.* **1998**, *74*, 1.
[33] $\Delta z_P < 0$, if the piezo device moves towards the cantilever.
[34] J. B. Pethica, A. P. Sutton, *J. Vac. Sci. Technol. A* **1988**, *6*, 2400.
[35] On a microscopic level, repulsion is a matter of overlapping wavefunctions of the tip and the sample according to Pauli's rule. Macroscopically, elastic restoring forces determine the behavior in this regime.
[36] It is assumed that the cantilever is not deformed. Although a transfer of material from the tip to the sample may occur, the condition is still valid, since common tips are made of Si_3N_4 or silicon oxide, which exhibit very high elastic modules (> 150 Gpa). For critical applications diamond cantilevers are available.
[37] N. A. Burnham, R. J. Colton, *Force Microscopy* in *Scanning Tunneling Microscopy and Spectroscopy* (Ed.: D. A. Bonnell), VCH, Weinheim, **1993**, p. 191.
[38] M. Mate, *Phys. Rev. Lett.* **1992**, *68*, 3323.
[39] M. Radmacher, M. Fritz, C. M. Kacher, J. P. Cleveland, P. K. Hansma, *Biophys. J.* **1996**, *70*, 556.
[40] S. R. Cohen, G. Neubauer, G. M. McClelland, *J. Vac. Sci. Technol. A* **1990**, *8*, 3449.
[41] B. Bhushan, V. N. Koinkar, *Appl. Phys.* **1994**, *64*, 1653.
[42] D. Krüger, B. Anczykowski, H. Fuchs, *Ann. Phys.* (*Leipzig*) **1997**, *6*, 341.
[43] J. L. Hutter, J. Bechhoefer, *Rev. Sci. Instrum.* **1993**, *64*, 1868.
[44] Along this line the slope is -1 and $\Delta d = 0$. Since the tip–sample distance does not change one sets $d = 0$ along the contact line.
[45] M. Rief, F. Oesterhelt, B. Heymann, H. E. Gaub, *Science* **1997**, *275*, 1295–1297.
[46] The tip and sample are made of the same material.
[47] The MYD/BHW theory not only considers surface forces but also deformations caused by them.[3]
[48] W. Mönch, G. Ertl, *Semiconductor surfaces and interfaces*, 2nd ed., Springer, Berlin, **1995.**
[49] Differences in the work function of the tip and the sample material lead to a contact potential. An electronic field between the tip and the sample can also occur as a result of patch charges on the surface. However, it is unlikely that electrostatic forces are the reason for

deviations in the long-range regime, since the data can be reasonably well described by a $1/d^2$ fit. Electrostatic forces would cause a slower decrease ($\propto 1/d$).
[50] H. W. Hao, A. M. Baró, J. J. Saenz, *J. Vac. Sci. Technol. B* **1991**, *9*, 1323.
[51] This is shown by the Hamaker constant of Si_3N_4: H(air, vacuum) = 16.71×10^{-20} J, H(water) = 6.07×10^{-20} J.
[52] R. J. Hunter, *Foundations of Colloid Science*, *Vol. I*, Oxford University Press, Oxford, **1993**.
[53] H.-J. Butt, E. K. Wolf, S. A. C. Gould, B. D. Northern, C. M. Peterson, P. K. Hansma, *J. Struct. Biol.* **1990**, *105*, 54.
[54] A. W. Adamson, *Physical Chemistry of Surfaces*, 5th ed., Wiley, New York, **1990**.
[55] A. L. Weisenhorn, P. Maivald, H.-J. Butt, P. K. Hansma, *Phys. Rev. B* **1992**, *45*, 45.
[56] P. Kékicheff, S. Marcelja, T. J. Senden, V. E. Shubin, *J. Chem. Phys.* **1993**, *99*, 6098.
[57] T. J. Senden, C. J. Drummond, P. Kékicheff, *Langmuir* **1994**, *10*, 358.
[58] T. J. Senden, C. J. Drummond, *Colloids Surf. A* **1995**, *94*, 29.
[59] A. Marti, G. Hähner, N. D. Spencer, *Langmuir* **1995**, *11*, 4632.
[60] X.-Y. Lin, F. Creuzet, H. Arribart, *J. Chem. Phys.* **1993**, *97*, 7272.
[61] Not only the dissolved ions but also the water dipoles screen the electrical field.
[62] V. A. Parsegian, D. Gingell, *Biophys. J.* **1972**, *12*, 1192.
[63] Double-layer repulsion belongs to the electrostatic forces.
[64] At low distances repulsive forces arising from the finite size of the solvent molecule occur. They are called structural or solvation forces.
[65] J. Gregory, *J. Colloid Interface Sci.* **1975**, *51*, 44.
[66] D. McCormack, S. L. Carnie, D. Y. Chan, *J. Colloid Interface Sci.* **1995**, *169*, 177.
[67] H.-J. Butt, *Biophys. J.* **1992**, *63*, 578.
[68] "Kraftspektroskopie: Von der van-der-Waals-Wechselwirkung zur Mechanik von Einzelmolekülen": M. Neitzert, Dissertation, Münster, **1999**.
[69] H.-J. Butt, *Biophys. J.* **1991**, *60*, 1438.
[70] A. Noy, D. V. Vezenov, C. M. Lieber, *Annu. Rev. Mater. Sci.* **1997**, *27*, 381 – 421.
[71] B. Capella, G. Dietler, *Surf. Sci. Rep.* **1999**, *34*, 1.
[72] H. Hertz, *J. Reine Angew. Math.* **1881**, *92*, 156.
[73] K. L. Johnson, K. Kendall, A. D. Roberts, *Proc. R. Soc. London A* **1971**, *324*, 301.
[74] B. V. Derjaguin, V. M. Muller, Y. P. Toporov, *J. Colloid Interface Sci.* **1975**, *53*, 314.
[75] a) V. M. Muller, V. S. Yushenko, B. V. Derjaguin, *J. Colloid Interface Sci.* **1980**, *77*, 91; b) B. D. Hughes, L. R. White Quart, *J. Mech. Appl. Math.* **1979**, *32*, 445.
[76] The measurement of γ_{ST} depends on the elastic deformation of tip and sample, which strictly speaking renders the independent determination of γ_{ST} impossible.
[77] a) H. Grubmüller, B. Heymann, P. Tavan, *Science* **1996**, *271*, 997; b) B. Heymann, H. Grubmüller, *Chem. Phys. Lett.* **1999**, *303*, 1.
[78] E. Evans, K. Ritchie, *Biophys. J.* **1997**, *72*, 1541.
[79] T. Han, J. M. Williams, T. P. Beebe, Jr., *Anal. Chim. Acta* **1995**, *307*, 365.
[80] G. I. Bell, *Science* **1978**, *200*, 618.
[81] G. U. Lee, L. A. Chrisey, R. J. Colton, *Science* **1994**, *266*, 771.
[82] A. Noy, D. V. Vezenov, J. F. Kayyem, T. J. Meade, C. Lieber, *Chem. Biol.* **1997**, *4*, 519.
[83] T. Boland, B. D. Ratner, *Proc. Natl. Acad. Sci. USA* **1995**, *92*, 5297.
[84] E.-L. Florin, M. Rief, H. Lehmann, M. Ludwig, C. Dornmair, V. T. Moy, H. E. Gaub, *Biosens. Bioelectron.* **1995**, *10*, 895.
[85] M. Rief, H. Clausen-Schaumann, H. E. Gaub, *Nat. Struct. Biol.* **1999**, *6*, 346.
[86] B. Essevaz-Roulez, U. Bockelmann, F. Heslot, *Proc. Natl. Acad. Sci. USA* **1997**, *94*, 11935.
[87] T. Strunz, K. Oroszlan, R. Schäfer, H. J. Güntherodt, *Proc. Natl. Acad. Sci. USA* **1999**, 96, 11277.
[88] U. Bockelmann, B. Essevaz-Roulet, F. Heslot, *Phys. Rev. Lett.* **1997**, *79*, 4489.
[89] U. Bockelmann, B. Essevaz-Roulet, F. Heslot, *Phys. Rev. E* **1998**, *58*, 2386.
[90] K. J. Breslauer, R. Frank, H. Blöcker, L. A. Marty, *Proc. Natl. Acad. Sci. USA* **1986**, 83, 3746.
[91] R. McKendry, M. E. Theoclitou, T. Rayment, C. Abell, *Nature* **1998**, *391*, 566.
[92] J. Fritz, A. G. Katopodis, D. Anselmetti, *Proc. Natl. Acad. Sci. USA* **1998**, *95*, 12283.
[93] M. Ludwig, V. T. Moy, M. Rief, E.-L. Florin, H. E. Gaub, *Microsc. Microanal. Microstruct.* **1994**, *5*, 321.
[94] For comparison: Florin et al.[4] determined a binding strength of F = 170 pN; Moy et al.[96] measured the value as F = 280 pN. This example illustrates that the binding strength is a matter of external conditions such as the pulling speed of the cantilever.
[95] U. Dammer, M. Hegner, D. Anselmetti, P. Wagner, M. Dreier, W. Huber, H.-J. Güntherodt, *Biopys. J.* **1996**, *70*, 2437.
[96] V. T. Moy, E. L. Florin, H. E. Gaub, *Colloids Surf.* **1994**, *93*, 343.
[97] "Kraftspektroskopie an Antikörper-Antigen-Systemen am Beispiel des Hb-A1c-Antikörpers": Y. Oberdörfer, Diplomarbeit, Münster, **1999**.
[98] M. Grandbois, M. Beyer, M. Rief, H. Clausen-Schaumann, H. E. Gaub, *Science* **1999**, *283*, 1727.
[99] H. Li, M. Rief, F. Oesterhelt, H. E. Gaub, *Adv. Mater.* **1998**, *3*, 316.
[100] F. Oesterhelt, M. Rief, H. E. Gaub, *New J. Phys.* **1999**, *1*, 6.1.
[101] In this section, attractive forces have positive values following the standard set in the literature.
[102] R. H. Austin, J. P. Brody, E. C. Cox, T. Duke, W. Volkmuth, *Phys. Today* **1997**, *50*, 32.
[103] L. R. G. Treloar, *The Physics of Rubber Elasticity*, 3rd ed., Oxford University Press, Oxford, **1975**.
[104] C. Bouchiat, M. D. Wang, J.-F. Allemand, T. Strick, S. M. Block, V. Croquette, *Biophys. J.* **1999**, *76*, 409.
[105] J. F. Marko, E. D. Siggia, *Macromolecules* **1995**, *28*, 8759.
[106] P.Cluzel, A. Lebrun, C. Heller, R. Lavery, J.-L. Viovy, D. Chatenay, F. Caron, *Science* **1996**, *271*, 792.
[107] T. Odijk, *Macromolecules* **1995**, *28*, 7016.
[108] S. B. Smith, Y. Cui, C. Bustamante, *Science* **1996**, *271*, 795.
[109] M. Rief, J. M. Fernandez, H. E. Gaub, *Phys. Rev. Lett.* **1998**, *81*, 4764.
[110] P. E. Marszalek, A. F. Oberhauser, Y.-P. Pang, J. M. Fernandez, *Nature* **1998**, *396*, 661.
[111] H. J. Kreuzer, R. L. C. Wang, M. Grunze, *New J. Phys.* **1999**, *1*, 21.1
[112] P. J. Flory, *Statistical Mechanics of Chain Molecules*, Hanser, München, **1988**.
[113] G. Strobl, *The Physics of Polymers*, 2nd ed., Springer, Berlin, **1997**.
[114] M. Doi, S. F. Edwards, *The Theory of Polymer Dynamics*, Oxford University Press, Oxford, **1998**.
[115] L. Harnau, P. Reineker, *New J. Phys.* **1999**, *1*, 3.1.
[116] C. Ortiz, G. Hadziioannou, *Macromolecules* **1999**, *32*, 780.
[117] H. Jensenius, G. Zocchi, *Phys. Rev. Lett.* **1997**, *79*, 5030.
[118] S. Chandrasekhar, *Rev. Mod. Phys.* **1943**, *15*, 1.
[119] The distribution function gives the probability that the end-to-end vector $\vec{x}$ points into a given volume element.
[120] H.-G. Elias, *An Introduction to Polymer Science*, 1st ed., VCH, Weinheim, **1997**.
[121] It is also conceivable that upon retraction of the cantilever the polymer becomes compressed, like tying a knot if the polymer is appropriately entangled.
[122] This is similar to the description of the paramagnetism or orientation of a dipole in an electrical field.
[123] Usually the extension $x(F)$ is plotted versus the force F and Equation (12) fitted to the experimental data.
[124] Equation (12) depicts an exact solution, while Equation (13) is an approximation for large values of n, which occurs in a common experiment. It is noteworthy that usually the distance x is varied and the force F measured. This procedure corresponds to Equation (13). The latest instruments permit the application of a particular force by magnetic cantilevers (A. Schemmel, H. E. Gaub, *Rev. Sci. Instrum.* **1999**, *70*, 1313).
[125] If $Fl_K \ll k_B T$ or $x \ll L$, then Equation (13) (FJC model) can be simplified to Equation (11), the GC model.
[126] T. J. Senden, J.-M. di Meglio, P. Auroy, *Eur. Phys. J. B* **1998**, *3*, 211.
[127] J. Fritz, A. G. Katopodis, F. Kolbinger, D. Anselmetti, *Proc. Natl. Acad. Sci. USA* **1998**, *95*, 12283.

[128] H. Kikuchi, N. Yokoyama, T. Kajiyama, *Chem. Lett.* **1997**, *11*, 1107.
[129] H. Li, W. Zhang, X. Zhang, J. Shen, B. Liu, C. Gao, G. Zou, *Macromol. Rapid Commun.* **1998**, *19*, 609.
[130] O. Kratky, G. Porod, *Recl. Trav. Chim.* **1949**, *68*, 1106.
[131] C. G. Baumann, S. B. Smith, V. A. Bloomfield, C. Bustamante, *Proc. Natl. Acad. Sci. USA* **1997**, *94*, 6185 – 6190.
[132] J. Kovac, C. G. Crabb, *Macromolecules* **1982**, *15*, 537.
[133] C. Bustamante, J. F. Marko, E. D. Siggia, S. B. Smith, *Science* **1994**, *265*, 1599.
[134] For a homogeneous slab (area momentum of inertia I, diameter Q) the connection between the bending module B and the elasticity module Y is given by: $B = IY = (\pi/32)Q^4Y$.
[135] S. B. Smith, L. Finzi, C. Bustamante, *Science* **1992**, *258*, 1122.
[136] C. Bouchiat, M. D. Wang, J.-F. Allemand, T. Strick, S. M. Block, V. Croquette, *Biophys. J.* **1999**, *76*, 409.
[137] M. Rief, M. Gautel, A. Schemmel, H. E. Gaub, *Biophys. J.* **1998**, *75*, 3008.
[138] M. Rief, J. Pascual, M. Saraste, H. E. Gaub, *J. Mol. Biol.* **1999**, *286*, 553.
[139] In the Gaussian regime the average of the square of the vector is given by $\langle \vec{x}^2 \rangle = L\, l_K = 2\, L\, l_P$.
[140] The specific stiffness Φ has the unit of a force and can be derived from the spring constant of the entire chain: $K = \Phi/L$. This approach is analogous to $K = \kappa/n$ in the case of the FJC model. Like the segment elasticity κ, Φ is also independent of the contour length. The relationship between κ and Φ is: $\Phi = \kappa/(n/L)$. The number of segments per length n/L is identical for all polymers of the same kind.
[141] M. D. Wang, H. Yin, R. Landick, J. Gelles, S. M. Block, *Biophys. J.* **1997**, *72*, 1335.
[142] The evaluation of Equation (16) in the form of the polynomial (left side) – (right side) = 0 is cumbersome, since only one of three possible solutions for F is useful.
[143] H. Li, M. Rief, F. Oesterhelt, H. E. Gaub, X. Zhang, J. Shen, *Chem. Phys. Lett.* **1999**, *305*, 197.
[144] a) A. Ashkin; J. M. Dziedzic, J. E. Bjorkholm, S. Chu, *Opt. Lett.* **1986**, *11*, 288; b) E.-L. Florin, A. Pralle, J. K. H. Hörber, E. H. K. Stelzer, *J. Struct. Biol.* **1997**, *119*, 202.
[145] J. F. Léger, G. Romano, A. Sarkar, J. Robert, L. Bourdieu, D. Chatenay, J. F. Marko, *Phys. Rev. Lett.* **1999**, 83, 1066.
[146] M. W. Konrad, J. I. Bolonick, *J. Am. Chem. Soc.* **1996**, 118, 10989.
[147] K. Kitamura, M. Tokunaga, A. H. Iwane, T. Yanagida, *Nature* **1999**, *397*, 129.
[148] U. Dammer, O. Popescu, P. Wagner, D. Anselmetti, H.-J. Güntherodt, G. M. Misevic, *Science* **1996**, 267, 1173.
[149] D. Müller, Jahrestagung der Gesellschaft für Biophysik, Ulm, **1999**.
[150] M. Benoit, D. Gabriel, G. Gerisch, H. E. Gaub, *Nature Cell Biol.* **2000**, *2*, 313.
[151] O. H. Willemsen, M. M. E. Snel, K. O. van der Werf, B. G. de Grooth, J. Greve, P. Hinterdorfer, H. J. Gruber, H. Schindler, Y. van Kooyk, C. G. Figdor, *Biophys. J.* **1998**, *75*, 2220.
[152] M. Rief, M. Gautel, F. Oesterhelt, J. M. Fernandez, H. E. Gaub, *Science* **1997**, *276*, 1109.
[153] A. F. Oberhauser, P. E. Marszalek, H. P. Erickson, J. M. Fernandez, *Nature* **1998**, *339*, 181.